

NASA/CR—2019-220065



Uncertainty Analysis of the CE-22 Advanced Nozzle Test Facility

Erin P. Hubbard
Jacobs Technology Inc., Cleveland, Ohio

March 2019

NASA STI Program . . . in Profile

Since its founding, NASA has been dedicated to the advancement of aeronautics and space science. The NASA Scientific and Technical Information (STI) Program plays a key part in helping NASA maintain this important role.

The NASA STI Program operates under the auspices of the Agency Chief Information Officer. It collects, organizes, provides for archiving, and disseminates NASA's STI. The NASA STI Program provides access to the NASA Technical Report Server—Registered (NTRS Reg) and NASA Technical Report Server—Public (NTRS) thus providing one of the largest collections of aeronautical and space science STI in the world. Results are published in both non-NASA channels and by NASA in the NASA STI Report Series, which includes the following report types:

- **TECHNICAL PUBLICATION.** Reports of completed research or a major significant phase of research that present the results of NASA programs and include extensive data or theoretical analysis. Includes compilations of significant scientific and technical data and information deemed to be of continuing reference value. NASA counter-part of peer-reviewed formal professional papers, but has less stringent limitations on manuscript length and extent of graphic presentations.
- **TECHNICAL MEMORANDUM.** Scientific and technical findings that are preliminary or of specialized interest, e.g., “quick-release” reports, working papers, and bibliographies that contain minimal annotation. Does not contain extensive analysis.
- **CONTRACTOR REPORT.** Scientific and technical findings by NASA-sponsored contractors and grantees.
- **CONFERENCE PUBLICATION.** Collected papers from scientific and technical conferences, symposia, seminars, or other meetings sponsored or co-sponsored by NASA.
- **SPECIAL PUBLICATION.** Scientific, technical, or historical information from NASA programs, projects, and missions, often concerned with subjects having substantial public interest.
- **TECHNICAL TRANSLATION.** English-language translations of foreign scientific and technical material pertinent to NASA's mission.

For more information about the NASA STI program, see the following:

- Access the NASA STI program home page at <http://www.sti.nasa.gov>
- E-mail your question to help@sti.nasa.gov
- Fax your question to the NASA STI Information Desk at 757-864-6500
- Telephone the NASA STI Information Desk at 757-864-9658
- Write to:
NASA STI Program
Mail Stop 148
NASA Langley Research Center
Hampton, VA 23681-2199

NASA/CR—2019-220065



Uncertainty Analysis of the CE-22 Advanced Nozzle Test Facility

Erin P. Hubbard
Jacobs Technology Inc., Cleveland, Ohio

Prepared under Contract NNC15BA02B

National Aeronautics and
Space Administration

Glenn Research Center
Cleveland, Ohio 44135

March 2019

Acknowledgments

This work was sponsored by the Aerosciences Evaluation and Test Capabilities (AETC) Portfolio at the NASA Glenn Research Center.

This report contains preliminary findings,
subject to revision as analysis proceeds.

Trade names and trademarks are used in this report for identification
only. Their usage does not constitute an official endorsement,
either expressed or implied, by the National Aeronautics and
Space Administration.

Level of Review: This material has been technically reviewed by NASA expert reviewer(s).

Available from

NASA STI Program
Mail Stop 148
NASA Langley Research Center
Hampton, VA 23681-2199

National Technical Information Service
5285 Port Royal Road
Springfield, VA 22161
703-605-6000

This report is available in electronic form at <http://www.sti.nasa.gov/> and <http://ntrs.nasa.gov/>

Contents

List of Figures	2
List of Tables	3
1 Abstract	4
2 Facility Description	6
3 Critical Measurements and Calculations	8
4 Calibrations and Corrections	10
5 Data Reduction Calculations	12
5.1 Thrust Stand Calibration	12
5.2 Tank pressure calibration	15
5.3 Secondary line calibration	16
5.4 Pressure tare calibration	17
5.5 ASME nozzle calibration	18
5.6 Customer test	18
6 Uncertainty approach	22
6.1 General Description	22
6.2 Elemental standard uncertainty estimates	23
6.2.1 Pressure measurements	23
6.2.2 Temperature measurements	24
6.2.3 Force measurements	25
6.2.4 Lengths and Areas	27
6.2.5 Regression Uncertainty	27
6.3 Summary of uncertainty inputs	29
7 Results	31
7.1 P_0 , PT , DP_{25} , NPR : Critical facility calculations	31
7.1.1 Random Uncertainty	31
7.1.2 Systematic and Combined uncertainty	32
7.2 M_{5ID} : Ideal Mach number at station 5	33
7.2.1 Random uncertainty	33
7.2.2 Systematic uncertainty	34
7.2.3 Combined uncertainty	35
7.3 FGY , FGZ , MX , MY , MZ : Gross forces and moments	36
7.3.1 Random uncertainty	36
7.3.2 Systematic uncertainty	36
7.3.3 Combined uncertainty	37
7.4 Uncertainty Sources	40
7.5 Example results for WP , CDN , FG and CFG : Mass flow, discharge coefficient, gross thrust and thrust coefficient	43
8 What-If Scenario	44
8.1 Push-Pull Calibration: Test Matrix Optimization	44
8.1.1 Scenario description	44
8.1.2 Scenario results	44
9 Conclusion	46
10 References	47

List of Figures

1	CE-22 test facility overview	6
2	Thrust stand and sign convention	7
3	Thrust stand with ASME nozzle installed	7
4	Airflow measurement locations for primary flow [1]	8
5	CE-22 calibration progression (from bottom to top)	10
6	Calibration flow chart	10
7	Thrust stand load cell locations and critical distances	12
8	Data Reduction summary for sensitivity matrices [S] and [U]	13
9	Summary of calculations to determine coefficients σ_{ij}	13
10	Summary of calculations to determine coefficients μ_{ij}	14
11	Push-pull calibration example	14
12	Tank pressure calibration data reduction flow chart	15
13	Tank pressure calibration example	15
14	Secondary line calibration data reduction flow chart	16
15	Secondary line pressure calibration example	16
16	Pressure tare calibration data reduction flow chart	17
17	Pressure tare (ALS3) calibration example	18
18	ASME nozzle calibration: <i>CF5C</i> data reduction flow chart	19
19	ASME nozzle calibration: <i>CD5C</i> data reduction flow chart	19
20	Data reduction flow chart for gross force along the <i>x</i> -axis	20
21	Data reduction flow chart for gross forces along the <i>y</i> - and <i>z</i> -axes and all gross moments	20
22	Data reduction flow chart for several airflow variables of interest	21
23	Instrumentation level uncertainty analysis flow	22
24	Systematic standard uncertainty estimate for ± 15 psid ESP system	24
25	Systematic standard uncertainty estimate for 45psid ESP system	24
26	Systematic standard uncertainty estimate for 500psid ESP system	24
27	Example of thrust stand force uncertainty determination for $b_{\mu_{4,2}}$ (see Figure 10)	26
28	ALS3 calibration/correction residuals and $s_{ALS3syx}$ uncertainty estimate	29
29	Synthetic error population example	29
30	Expanded random uncertainty and UPC contributing to S_{NPR} for $PT = 45$ psia	32
31	Expanded combined uncertainty for $P0$, PT , $DP25$, and NPR (U_{NPR} shown for $PT = 45$ psia)	32
32	Expanded combined uncertainty in NPR for various PT settings	33
33	Random UPC contributing to S_{M5ID} for various nozzle sizes	34
34	Expanded random uncertainty and UPC contributing to S_{M5ID} for 40in ² nozzle	34
35	Expanded systematic uncertainty, B_{M5ID} , for various nozzle sizes	35
36	Expanded combined uncertainty, U_{M5ID} , for various nozzle sizes	35
37	UPC to random uncertainties in gross forces and moments	36
38	Expanded systematic uncertainty in directional gross forces FGY and FGZ	37
39	Expanded systematic uncertainty in moments	37
40	Expanded combined uncertainty in gross forces FGY and FGZ	38
41	Expanded combined uncertainty in calculated moments	38
42	Tabulated results for expanded random, systematic and combined uncertainty in FGY , FGZ , MX , MY and MZ	39
43	Uncertainty sources and their levels of contribution to u_{P0} , u_{PT} , u_{DP25} , u_{MX} , u_{MY} , u_{MZ} , and u_{M5ID}	40
44	Uncertainty sources and their levels of contribution to u_{NPR}	41
45	Uncertainty sources and their levels of contribution to u_{FGY} and u_{FGZ}	42
46	Example of expanded combined, random and systematic uncertainty in critical variables of interest	43
47	Expanded systematic uncertainty in MX for proposed Push-Pull calibration test matrices	45
48	Expanded systematic uncertainty in MY for proposed Push-Pull calibration test matrices	45
49	Expanded systematic uncertainty in MZ for proposed Push-Pull calibration test matrices	45

List of Tables

1	Critical Measurements	9
2	Critical Calculations	9
3	Calibration descriptions and corrections determined	11
4	Elemental uncertainty estimates for ESP pressure measurements	23
5	Elemental uncertainty estimates for differential pressure measurements (<i>DP25</i>)	25
6	Elemental uncertainty estimates for thermocouple measurements (<i>TT</i>)	25
7	Systematic standard uncertainty estimates for load combinations corresponding to the [S] ⁻¹ matrix	26
8	Systematic standard uncertainty estimates for load combinations corresponding to the [U] ⁻¹ matrix	26
9	Elemental systematic standard uncertainty estimates for lengths and areas	27
10	Uncertainties associated with predicting values from Tank Pressure (<i>P0</i>) linear calibration fits	28
11	Uncertainties associated with predicting values from Secondary Line linear calibration fits	28
12	Summary of inputs to uncertainty propagation	30
13	Expanded random uncertainty in critical facility pressures <i>P0</i> , <i>PT</i> , and <i>DP25</i>	31
14	Expanded random uncertainty in <i>M5ID</i> for various nozzle sizes (estimates valid across all <i>NPR</i>)	33
15	Expanded random uncertainty in gross forces and moments	36

1 Abstract

This paper presents methods and results of a detailed measurement uncertainty analysis that was performed for the Advanced Nozzle Test Facility, CE-22, located at the NASA Glenn Research Center. Results for the uncertainty in thrust and flow coefficients in addition to other variables of interest are provided. Results are presented separately as random uncertainty (characterizing errors inherent to instrument or measurement environment, impacting repeatability), systematic uncertainty (capturing inaccuracies due to measurement process, calibration, installation effects or other similar sources which may introduce bias), and total combined uncertainty. The statistical methods and engineering judgments used to estimate elemental uncertainties are described. MANTUS (Measurement ANalysis Tool for Uncertainty in Systems) was used to quantify instrumentation uncertainty, and statistical analysis and engineering judgment were used to quantify other random and systematic uncertainty sources. The Monte Carlo method was used to propagate systematic and random elemental uncertainties to determine the uncertainties of various calculated variables of interest.

Nomenclature

γ	Specific heat ratio for air (1.4)
A	Area, in ²
B_x	Expanded systematic uncertainty of variable x
b_x	Systematic standard uncertainty of variable x
CDN	Nozzle discharge coefficient
CFG	Thrust coefficient
CX, CY, CZ	Thrust stand calibration loads, lbf
DP	Differential pressure, psid
$DP0, \Delta P0$	Change in tank pressure, psid
FG	Gross force, lbf
FX, FY, FZ	Directional forces on the nozzle, lbf
L	Length, inches
$M5ID, M5$	Ideal and corrected Mach number at station 5
MX, MY, MZ	Moments acting on the nozzle, lbf-in
NPR	Nozzle pressure ratio $PT/P0$
$P0$	Tank pressure, psia
PS	Static pressure, psia
$PS3QP0$	Pressure ratio $PS3/P0$
PT	Total pressure, psia
RX, RY, RZ	Thrust stand reaction loads, lbf
S_x	Expanded random uncertainty of variable x
s_x	Random standard uncertainty of variable x
s_{yx}	Standard error of estimate; used to quantify regression uncertainty
TT	Total Temperature, °R
U_x	Expanded combined uncertainty of variable x
WP	Weight flow for primary flow stream, lbm/s
[S],[U]	Thrust stand sensitivity matrices
MANTUS	Measurement Analysis Tool for Uncertainty in Systems
MCM	Monte Carlo Method
TSM	Taylor Series Method

2 Facility Description

CE-22 houses the Advanced Nozzle Test Facility test rig, located within the Engine Research Building at NASA Glenn Research Center in Cleveland, Ohio (Figure 1). Nozzle performance characteristics for nozzles ranging from 6 to 40 square inch throat areas are determined by measurements from a 3-axis thrust stand (Figure 2) and several probes within the test rig[1].

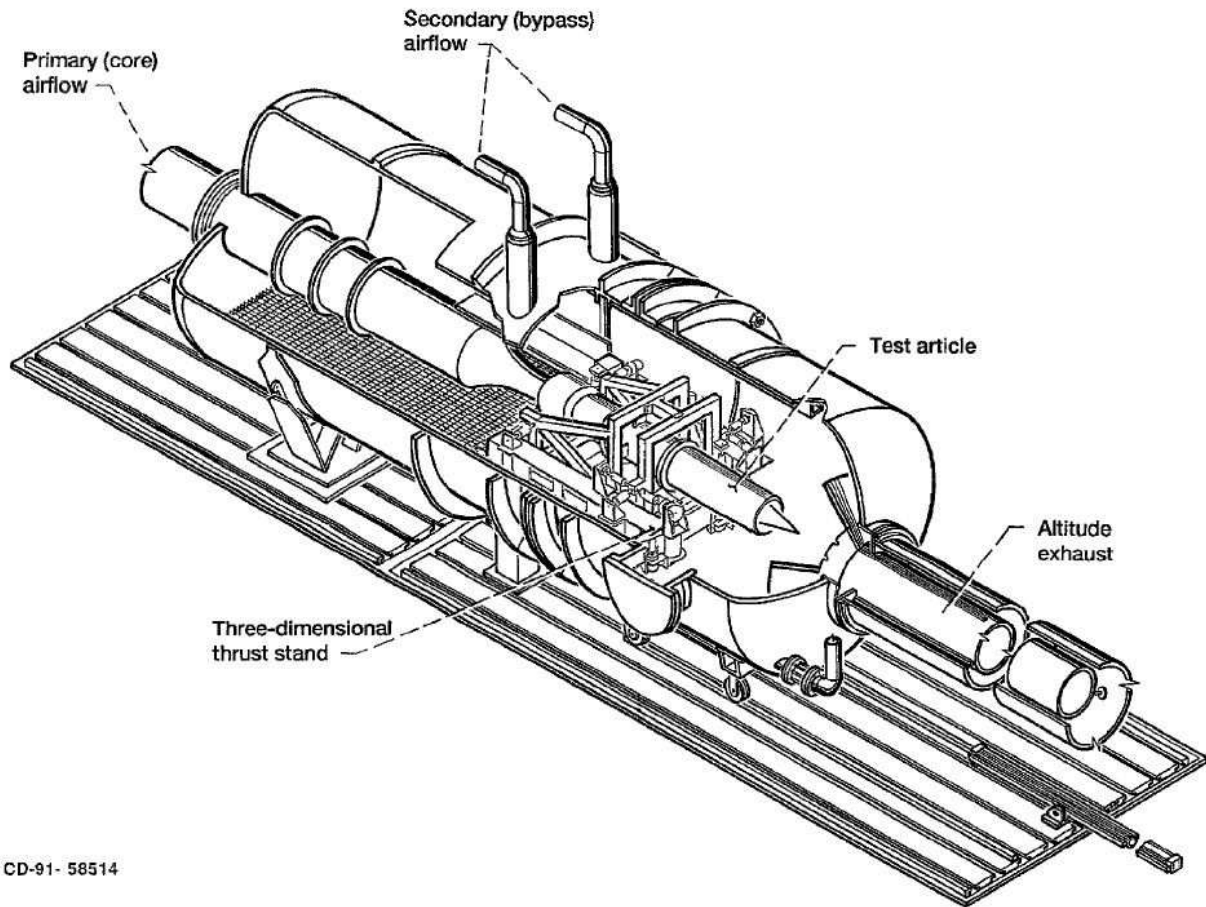


Figure 1: CE-22 test facility overview [2]

The facility can achieve nozzle pressure ratios up to 50 while simulating altitudes from sea level to 48,000 feet. It also has various configuration options (swirl vane package, specific calibrations for nozzle sizes, various ranges of differential pressure transducers installed, etc.). For the purpose of this analysis, which quantifies uncertainty on a general facility scale, the most standard facility configurations are assumed.^a Figure 3 shows the thrust stand with an ASME nozzle installed.

^aStandard facility configuration parameters: no swirl vane installed, full range ASME calibration, highest range differential pressure transducers installed (5 psid), no secondary line usage.

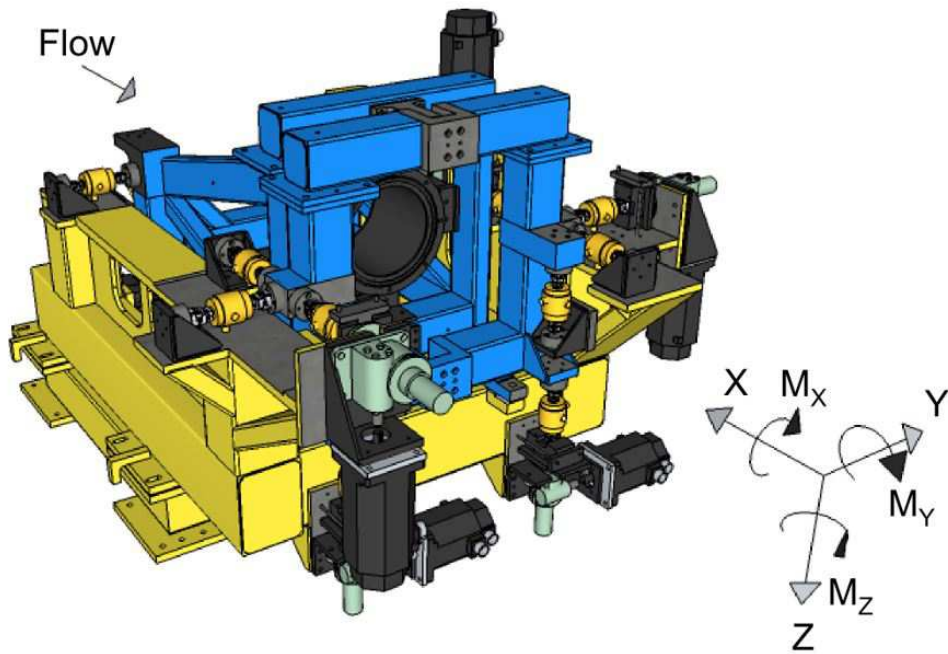


Figure 2: Thrust stand and sign convention [2]



Figure 3: Thrust stand with ASME nozzle installed [3]

3 Critical Measurements and Calculations

Often times hundreds or even thousands of measurements are taken in test facilities; some for facility health monitoring, some for operations, some for redundancy, and some for calculation of key variables and critical parameters. Figure 4 shows the station locations and arrangement of key measurements in this facility. Tables 1 and 2 further describe key facility variables and the measurements upon which they rely.

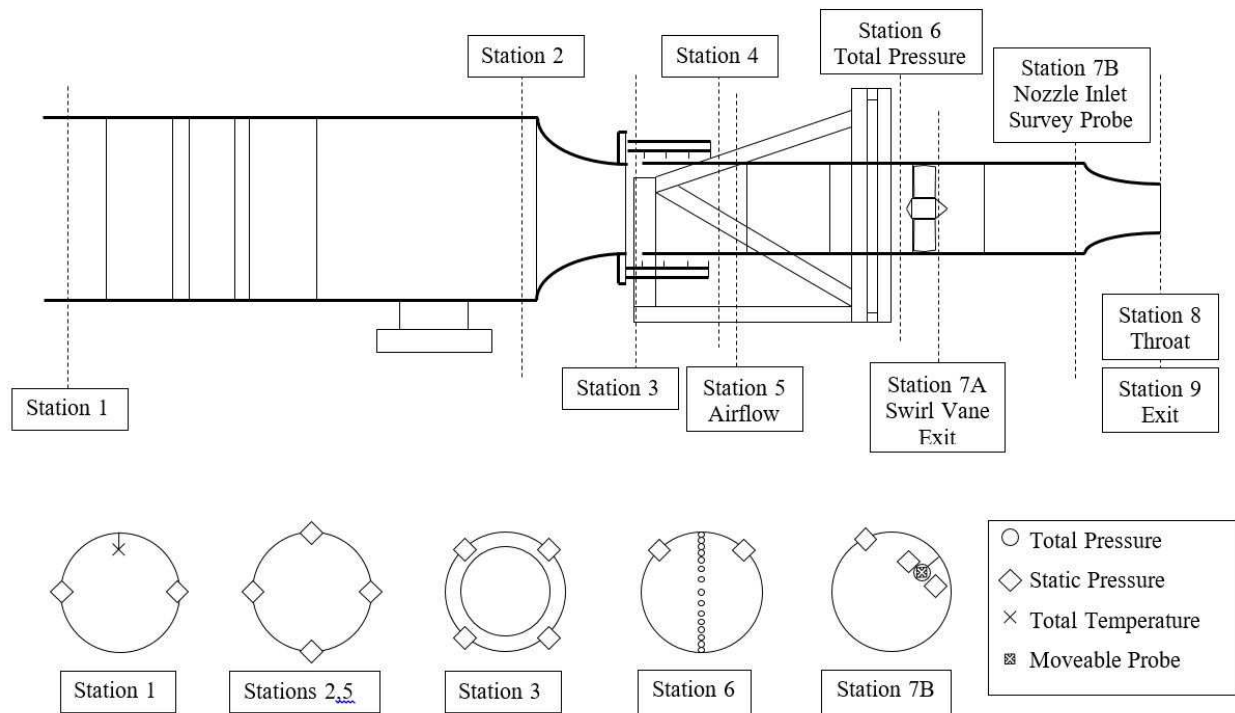


Figure 4: Airflow measurement locations for primary flow [1]

Variable Name	Description	Number of measurements	Instrumentation
<i>P0</i>	Ambient tank pressure, psia	2	ESP, 15psi range
<i>PT</i>	Total pressure ^b , psia	15	ESP, 45psi range
<i>DP25</i>	Bellmouth differential pressure, psid	4	Sensotec or Bell & Howell 1,2 or 5psid ^c
<i>PS1, PS2, PS3, PS5, PS6</i>	Static pressure at various stations, psia	2, 4, 4, 4, 2, respectively	ESP, 45psi range
<i>PS302, PS303</i>	Secondary line pressures, psia	1 per line	ESP, 500psi range
<i>TT</i>	Total temperature in primary flow, °R	5	Type K thermocouple, reference oven
<i>RX, RY, RZ</i>	Reaction loads, lbf	2, 2, 4, respectively	2,000 and 4,000 lbf load cells
<i>CX, CY, CZ</i>	Calibration loads, lbf	2, 2, 4, respectively	2,000 and 4,000 lbf load cells
<i>LY, LR, LP1, LP2</i>	Thrust stand moment arms to load cell locations	n/a	Facility provided
<i>A5, ALS1</i>	Area at station 5 and labyrinth seal area, in ²	n/a	Facility provided
<i>A8</i>	Nozzle exit area, in ²	n/a	Customer provided (unless ASME)

Table 1: Description of critical measurements

Variable Name	Description	$f(x)$
<i>NPR</i>	Nozzle pressure ratio for primary stream	$f(PT, P0)$
<i>M5ID</i>	Ideal Mach number for primary stream	$f(PS1, DP25)$
<i>WP</i>	Weight flow for primary stream, lbm/sec	$f(A5, P0, PS1, TT6, DP25)$
<i>FGX</i>	Gross axial force on the nozzle, lbf	$f(RX, RY, RZ, PS302, PS303, P0, PT, PS1, PS3, PS5, PS6, DP25)$
<i>FGY, FGZ</i>	Gross off-axis directional forces on the nozzle, lbf	$f(RX, RY, RZ, PS302, PS303, P0)$
<i>MX, MY, MZ</i>	Moments acting on the nozzle, lbf-in	$f(RX, RY, RZ, PS302, PS303, P0)$
<i>FG</i>	Gross force on the nozzle, lbf	$f(FGX, FGY, FGZ)$
<i>CDN</i>	Nozzle discharge coefficient	$f(A8, WP, M5ID, PT, TT, \gamma)$
<i>CFG</i>	Thrust coefficient	$f(FG, WP, TT, NPR, \gamma)$

Table 2: Description of critical calculated variables

^bThis value is corrected if swirl vane package is used; since this is not a standard configuration, this uncertainty analysis does not include this correction.

^cDepending on the test matrix and nozzle sizes being tested, *DP25* configuration may vary. For this analysis, 5 psid Bell & Howell transducer installation is assumed.

4 Calibrations and Corrections

A series of calibrations is performed to determine corrections for incidental forces that act upon the thrust stand in order to isolate thrust produced by the test article. Figure 5 shows the calibration progression sequence, from bottom to top. Figure 6 additionally shows which calibrations are nested within one another, which is particularly important to understand when considering the impact of how uncertainty from a calibration propagates through subsequent calibrations and ultimately impacts the customer test. Note that the deadweight check visible in Figure 5 is merely a verification of some of the sensitivity matrix results. While it is an important step procedurally for verification, it does not impact the calculations of variables of interest and is therefore not incorporated into this analysis.

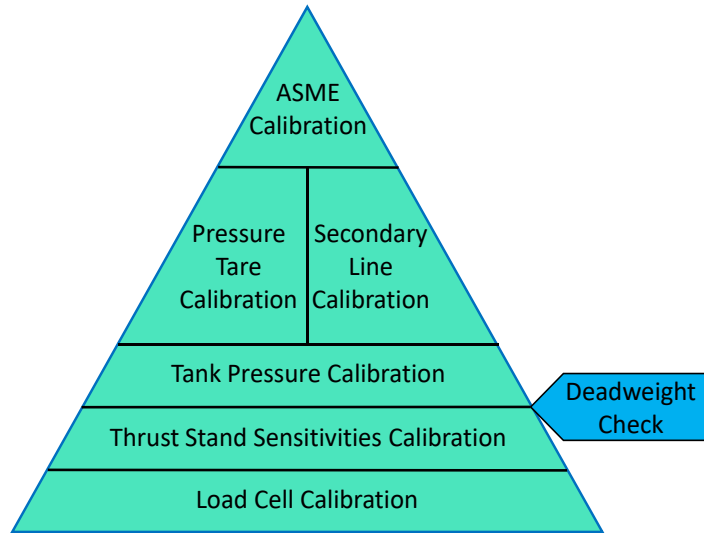


Figure 5: CE-22 calibration progression (from bottom to top)

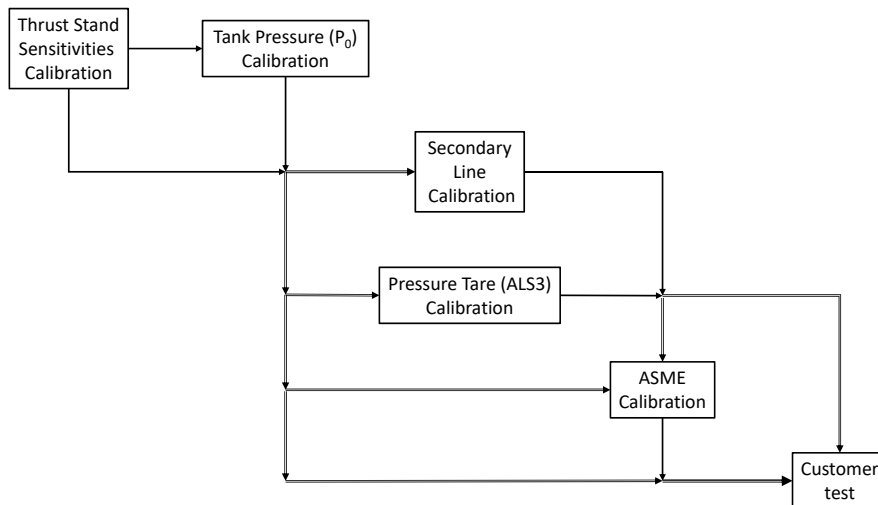


Figure 6: Calibration flow chart

Table 3 summarizes the calibrations and the resulting corrections, which are fully detailed in other publications[2][3][1].

Calibration Name	Description	Calibrated values or correction factors determined
Thrust stand sensitivities (“Push-Pull”) calibration	Various forces are applied to the thrust stand by calibration load cells (<i>CX, CY, CZ</i>) inducing forces and moments in various directions experienced by the thrust stand reaction load cells (<i>RX, RY, RZ</i>). Sensitivities to loads are determined by the slopes of the reaction vs. calibration forces.	Sensitivity matrices [S] and [U] are used to calculate directional forces and moments
Tank Pressure (“P0”) calibration	When the tank vacuums out to low pressure, tank deflections exert incidental forces observed by the thrust stand. Sensitivities to change in tank pressure ($\Delta P0$) are determined by closing off the tank exhaust and finding slopes of reaction loads vs. $\Delta P0$	<i>FXP0, FYP0, FZP0, MXP0, MYP0, MZP0</i>
Secondary line calibration	Customers have the option to use secondary lines during testing. This correction is determined to assure any forces exerted through use of the secondary flow lines are accounted for. Sensitivities to difference in pressure between the secondary line pressures and tank pressure are determined by capping off the secondary line pipes and finding slopes of reaction loads vs. $\Delta P5302C0$ and $\Delta P5303C0$	<i>FX302, FX303, FY302, FY303, FZ302, FZ303, MX302, MX303, MY302, MY303, MZ302, MZ303</i>
Pressure tare calibration (“ADP”, “ $\Delta\Delta P$ ”, “ALS3”)	A correction is determined which accounts for the frictional force acting on the primary duct as air exits through the labyrinth seal. This correction is determined by blanking off the duct just downstream of the labyrinth seal at station 5, pressurizing the main line, and analyzing the reaction loads.	<i>FTARE</i>
ASME calibration	The ASME calibration is performed to form a relationship between thrust stand reactions and known nozzle characteristic behavior. During a customer test, the nozzle performance can be determined through commonalities between the tested nozzle and known ASME nozzle performance.	<i>CD5, CF5</i>

Table 3: Calibration descriptions and corrections determined

5 Data Reduction Calculations

The data reduction sequence from raw measurements through the calculation of critical variables of interest must be well understood and replicated within the Monte Carlo code environment in order to propagate uncertainties properly. This section describes the data reduction for each test performed in CE-22 leading to and including a customer test. Data reduction flow charts were developed for all tests to aid the engineer in tracking these calculations while developing the code. They are included in this report to depict the route from raw measurements to variables of interest, as well as to show the sheer number of measurements that are included in final calculations of critical variables.

5.1 Thrust Stand Calibration

For a perfect thrust stand, the applied loads would be exactly equal and in opposite direction to the reaction loads. However, as with any physical system, imperfections lead to off-axis loading, hysteresis, non-linearity and other effects. This calibration is meant to account for some of these imperfections so that directional forces can be predicted from thrust stand reaction loads.

A series of loads exerted by the calibration load cells induce directional forces and moments on the thrust stand. Sensitivities are developed when those exerted loads are plotted against the observed reaction loads and first order curves are fit to the data. Figure 7 shows the locations of calibration and reaction load cells. Figure 8 shows a flow chart summary of the data reduction to obtain the load sensitivities. Figures 9 and 10 summarize the equations used to obtain all σ and μ values (slopes of the first order fits to calibration data). A full and detailed description of the test matrix and data reduction sequence, as well as the derivation of the sensitivity matrices $[S]$ and $[U]$, can be found in reference [3].

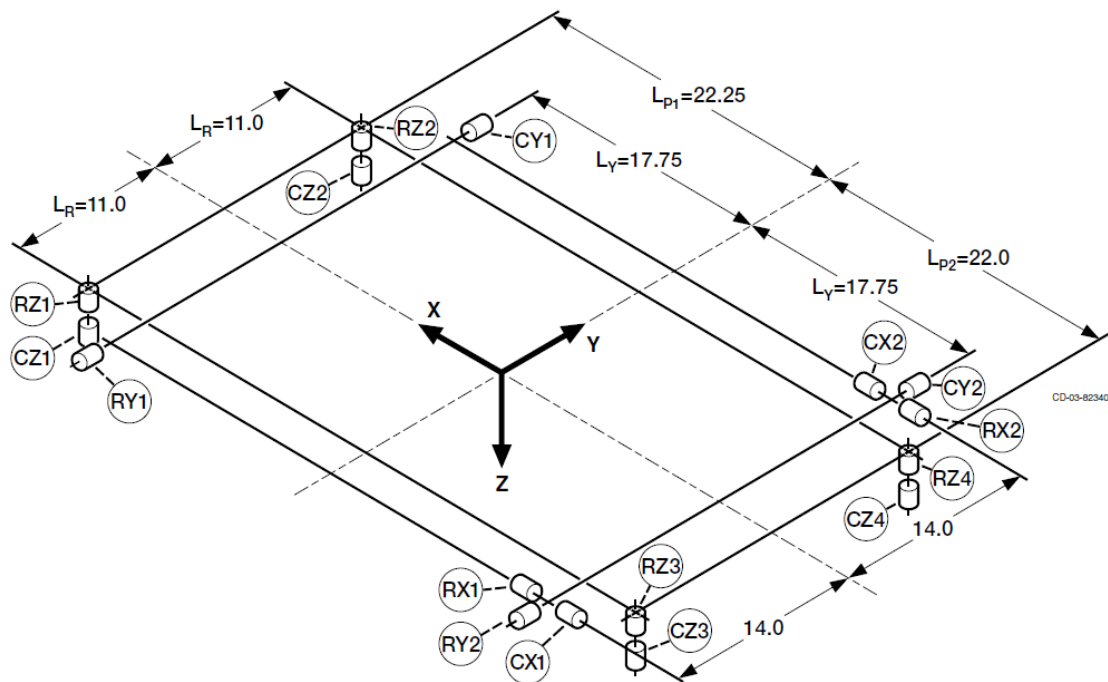


Figure 7: Thrust stand load cell locations and critical distances [3]

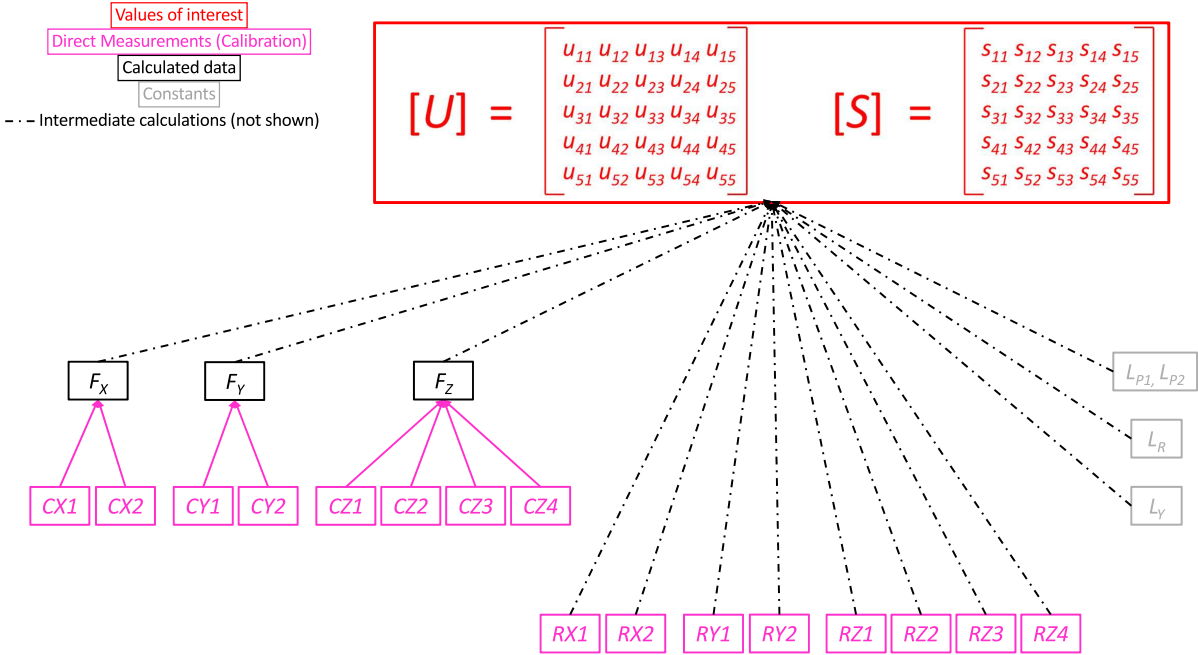


Figure 8: Data Reduction summary for sensitivity matrices [S] and [U]

$i \setminus j$	1	2	3	4	5
1	$\frac{\Delta(RX1+RX2)}{\Delta FX}$	$\frac{\Delta(RX1+RX2)}{\Delta FY}$	$\frac{\Delta(RX1+RX2)}{\Delta FZ}$	$\frac{1}{L_R} \left(\frac{\Delta(RX1+RX2)}{\Delta FZ} - \sigma_{13} \right)$	$\frac{1}{L_Y} \left(\frac{\Delta(RX1+RX2)}{\Delta FY} - \sigma_{12} \right)$
2	$\frac{\Delta RY1}{\Delta FX}$	$\frac{\Delta RY1}{\Delta FY}$	$\frac{\Delta RY1}{\Delta FZ}$	$\frac{1}{L_R} \left(\frac{\Delta RY1}{\Delta FZ} - \sigma_{23} \right)$	$\frac{1}{L_Y} \left(\frac{\Delta RY1}{\Delta FY} - \sigma_{22} \right)$
3	$\frac{\Delta RY2}{\Delta FX}$	$\frac{\Delta RY2}{\Delta FY}$	$\frac{\Delta RY2}{\Delta FZ}$	$\frac{1}{L_R} \left(\frac{\Delta RY2}{\Delta FZ} - \sigma_{33} \right)$	$\frac{1}{L_Y} \left(\frac{\Delta RY2}{\Delta FY} - \sigma_{32} \right)$
4	$\frac{\Delta(RZ1+RZ3)}{\Delta FX}$	$\frac{\Delta(RZ1+RZ3)}{\Delta FY}$	$\frac{\Delta(RZ1+RZ3)}{\Delta FZ}$	$\frac{1}{L_R} \left(\frac{\Delta(RZ1+RZ3)}{\Delta FZ} - \sigma_{43} \right)$	$\frac{1}{L_Y} \left(\frac{\Delta(RZ1+RZ3)}{\Delta FY} - \sigma_{42} \right)$
5	$\frac{\Delta(RZ2+RZ4)}{\Delta FX}$	$\frac{\Delta(RZ2+RZ4)}{\Delta FY}$	$\frac{\Delta(RZ2+RZ4)}{\Delta FZ}$	$\frac{1}{L_R} \left(\frac{\Delta(RZ2+RZ4)}{\Delta FZ} - \sigma_{53} \right)$	$\frac{1}{L_Y} \left(\frac{\Delta(RZ2+RZ4)}{\Delta FY} - \sigma_{52} \right)$

Figure 9: Summary of calculations to determine coefficients σ_{ij} for the $[S]^{-1}$ matrix [3]

$i \setminus j$	1	2	3	4	5
1	$\frac{\Delta(RX1+RX2)}{\Delta FX}$	$\frac{\Delta(RX1+RX2)}{\Delta FY}$	$\frac{\Delta(RX1+RX2)}{\Delta FZ}$	$\frac{1}{L_P} \left(\frac{\Delta(RX1+RX2)}{\Delta FZ} - \mu_{13} \right)$	$\frac{1}{L_Y} \left(\frac{\Delta(RX1+RX2)}{\Delta FY} - \mu_{12} \right)$
2	$\frac{\Delta RY1}{\Delta FX}$	$\frac{\Delta RY1}{\Delta FY}$	$\frac{\Delta RY1}{\Delta FZ}$	$\frac{1}{L_P} \left(\frac{\Delta RY1}{\Delta FZ} - \mu_{23} \right)$	$\frac{1}{L_Y} \left(\frac{\Delta RY1}{\Delta FY} - \mu_{22} \right)$
3	$\frac{\Delta RY2}{\Delta FX}$	$\frac{\Delta RY2}{\Delta FY}$	$\frac{\Delta RY2}{\Delta FZ}$	$\frac{1}{L_P} \left(\frac{\Delta RY2}{\Delta FZ} - \mu_{33} \right)$	$\frac{1}{L_Y} \left(\frac{\Delta RY2}{\Delta FY} - \mu_{32} \right)$
4	$\frac{\Delta(RZ1+RZ2)}{\Delta FX}$	$\frac{\Delta(RZ1+RZ2)}{\Delta FY}$	$\frac{\Delta(RZ1+RZ2)}{\Delta FZ}$	$\frac{1}{L_P} \left(\frac{\Delta(RZ1+RZ2)}{\Delta FZ} - \mu_{43} \right)$	$\frac{1}{L_Y} \left(\frac{\Delta(RZ1+RZ2)}{\Delta FY} - \mu_{42} \right)$
5	$\frac{\Delta(RZ3+RZ4)}{\Delta FX}$	$\frac{\Delta(RZ3+RZ4)}{\Delta FY}$	$\frac{\Delta(RZ3+RZ4)}{\Delta FZ}$	$\frac{1}{L_P} \left(\frac{\Delta(RZ3+RZ4)}{\Delta FZ} - \mu_{53} \right)$	$\frac{1}{L_Y} \left(\frac{\Delta(RZ3+RZ4)}{\Delta FY} - \mu_{52} \right)$

Figure 10: Summary of calculations to determine coefficients μ_{ij} for the $[\mathbf{U}]^{-1}$ matrix [3]

An example of two plots produced from the Push-Pull calibration data (and subsequent slope/sensitivity determination using least-squares linear fits) is shown in Figure 11. This particular example shows the sensitivity of response loads in the x- and y-directions ($RX1+RX2$, $RY2$) when x-directional forces are applied by calibration load cells ($FX_{applied} = CX1 + CX2$). These plots show both on- and off-axis reaction sensitivities; ideally, on-axis slopes would be equivalent to 1 and off-axis would be 0. But as was previously mentioned, the thrust stand is an imperfect physical system which is characterized by this calibration. The slope from the on-axis reaction load analysis falls into both the $[\mathbf{S}]^{-1}$ and $[\mathbf{U}]^{-1}$ matrices' upper left hand entry, $\sigma_{1,1}$ and $\mu_{1,1}$, while the off-axis slope shown from the $RY2$ reaction load falls into $\sigma_{3,1}$ and $\mu_{3,1}$ (see Figures 9 and 10). The rest of the $[\mathbf{S}]^{-1}$ and $[\mathbf{U}]^{-1}$ matrices are filled out with similar reaction load analyses.

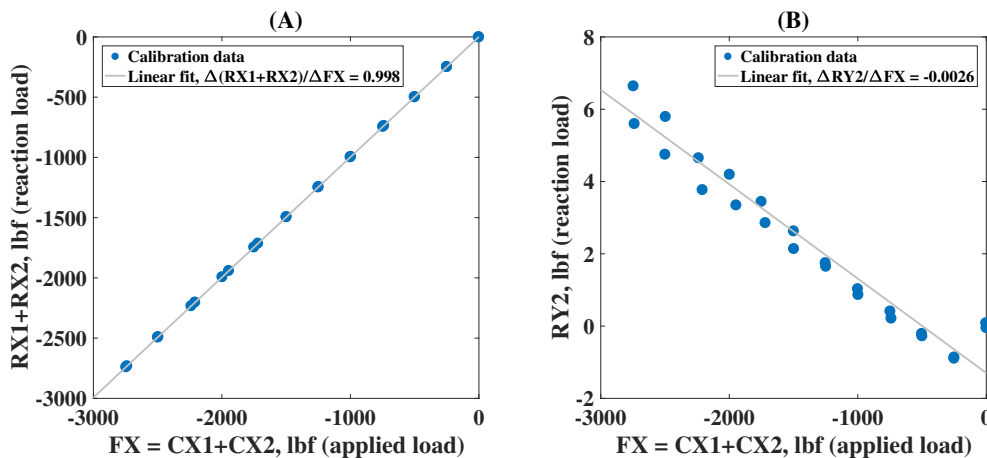


Figure 11: Push-pull calibration: Example determinations of on- (A) and off-axis (B) reaction load sensitivities for $[\mathbf{S}]^{-1}$ and $[\mathbf{U}]^{-1}$ matrices (i.e., $\sigma_{1,1} = \mu_{1,1} = 0.998$ and $\sigma_{3,1} = \mu_{3,1} = 0. - 0.0026$)

5.2 Tank pressure calibration

Since the thrust stand is mounted directly to the large outer pressure tank in the facility, minor deflections due to change in tank pressure (ΔP_0) cause incidental forces to be observed by the thrust stand. Sensitivities from the $[S]$ and $[U]$ matrices previously determined are fed into this data reduction, depicted in Figure 12. Correction coefficients are determined by plotting reaction loads and moments versus change in tank pressure, ΔP_0 . An example of this for determination of slope $CFXP_0$ is shown in Figure 13.

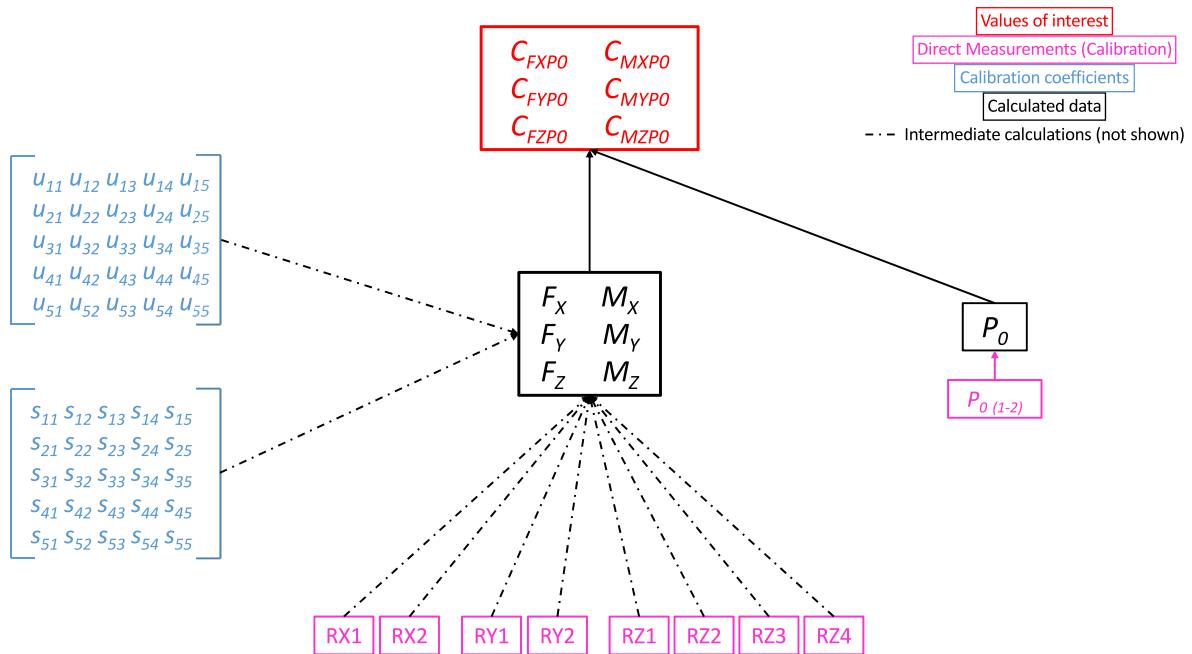


Figure 12: Tank pressure calibration data reduction flow chart

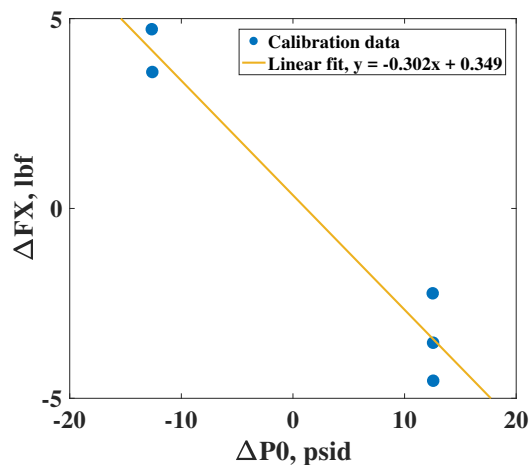


Figure 13: Tank pressure calibration: Example determination of sensitivity coefficient for FXP_0 ($CFXP_0 = -0.302\text{lbf/psi}$)

5.3 Secondary line calibration

Use of the 450psia secondary air lines cause loads to be exerted on the thrust stand. To account for this, correction coefficients are determined by plotting the reaction loads and moments versus the secondary line air pressures $PS302C$ and $PS303C$. Sensitivities from the $[S]$ and $[U]$ matrices as well as correction coefficients previously determined from the tank pressure calibration are fed into this data reduction, depicted in Figure 14. An example of this is shown in Figure 15 for determination of $CFXP302$.

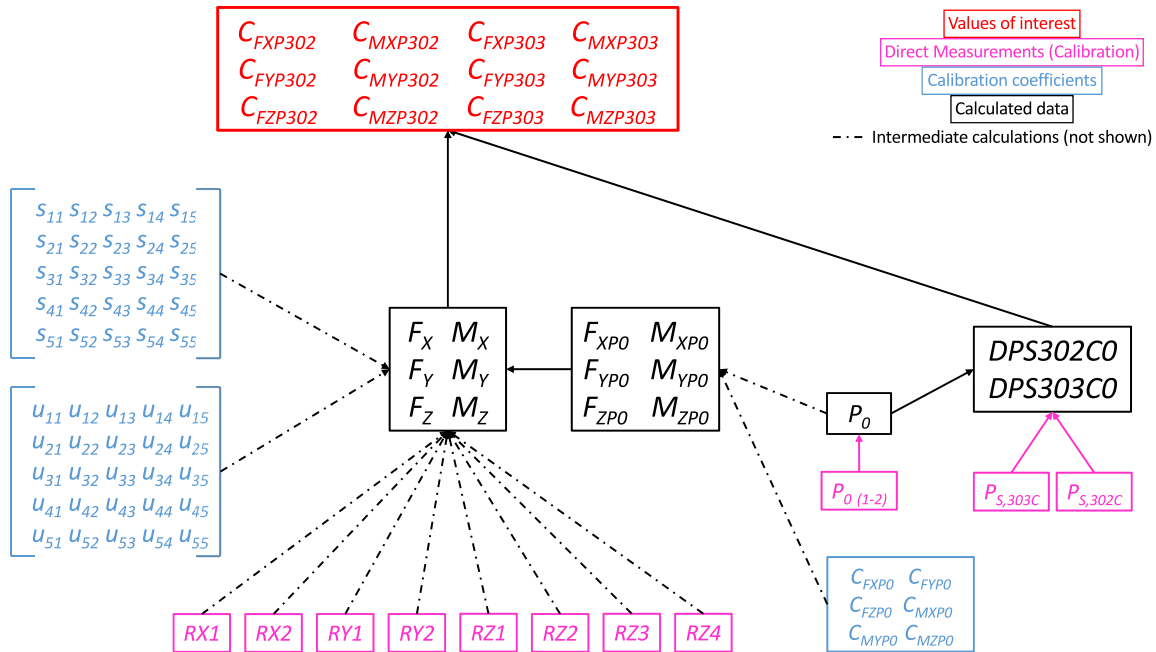


Figure 14: Secondary line calibration data reduction flow chart

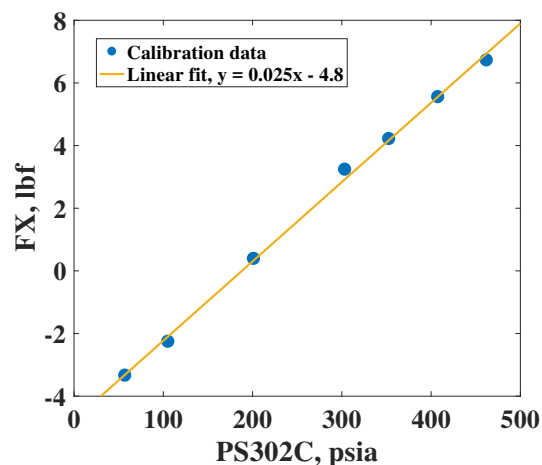


Figure 15: Secondary line pressure calibration: Example determination of sensitivity coefficient for $FX302$ ($CFXP302C = 0.025\text{lbf/psi}$)

5.4 Pressure tare calibration

A small gap exists between a labyrinth seal and the main supply airflow duct in CE-22 so that the thrust stand remains free-floating. When a difference in air pressure is present between the tank and airflow duct, a small amount of air flows through this space, exerting a frictional force on the test article detected by reaction loads on the thrust stand. The “ALS3” or “pressure tare” calibration determines corrections for this incidental friction force using the Nelder-Mead method as a least squares minimizing function, factoring in several variables such as total pressure at station 6 (PT_6), static pressure ratio PS_3QP_0 , and a calculated “effective area” ($ALS_{3measured}$). Sensitivities from the $[U]$ matrix determined from the push-pull calibration, as well as correction coefficient $CFXP_0$ previously determined from the tank pressure calibration, are fed into this data reduction sequence in addition to several other facility measurements, as depicted in Figure 16. An example of the pressure tare calibration fits at various total pressures is shown in Figure 17.

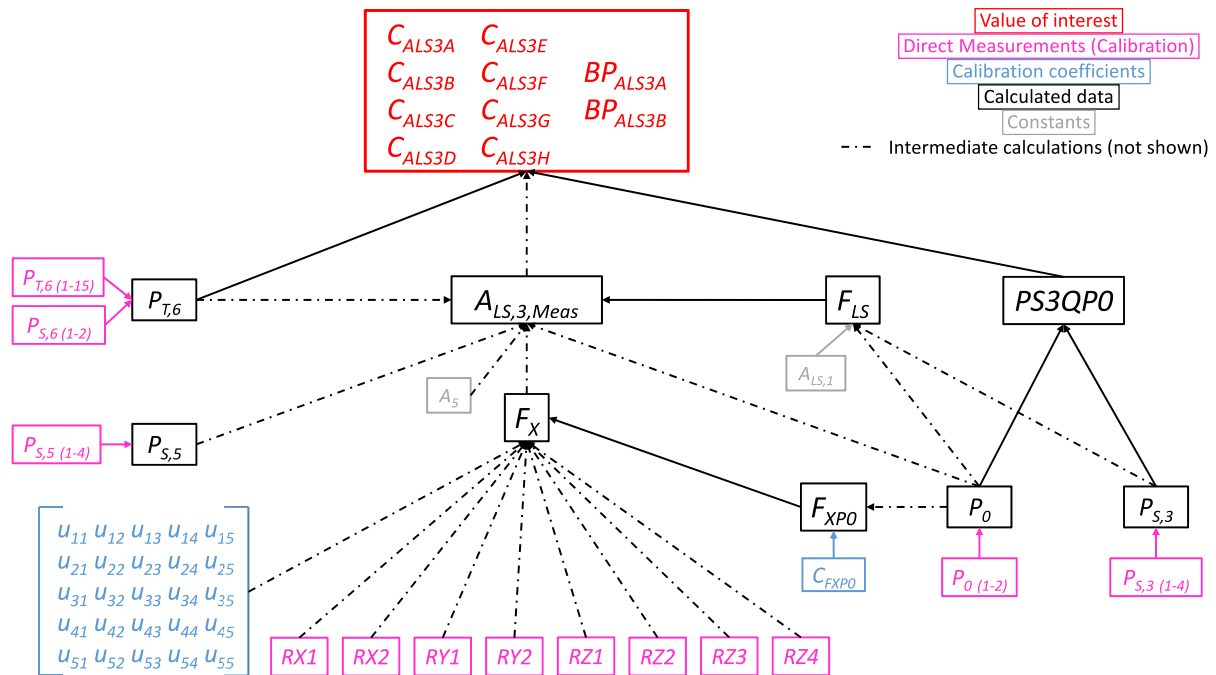


Figure 16: Pressure tare calibration data reduction flow chart

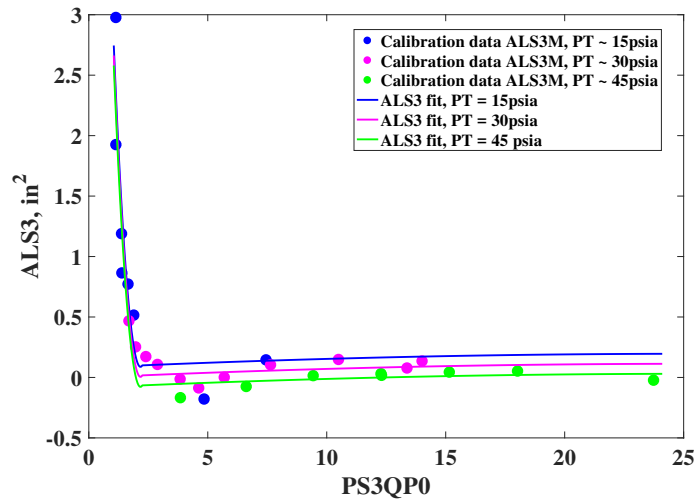


Figure 17: Pressure tare calibration: Example of ALS3 data and calibration curves at various total pressures

5.5 ASME nozzle calibration

The typical calibration sequence in CE-22 ends with the ASME nozzle calibration, which captures thrust stand reaction to known nozzle behavior. The Nelder-Mead method is used as a least squares minimizing function to develop a set of curve-fits for predicting nozzle discharge ($CD5$) and gross thrust coefficients ($CF5$) at station 5. Input data for this function in developing $CD5$ coefficients are $PS3QP0$, $M5ID$, and $CD5C$. Input data for developing $CF5$ coefficients are $PS3QP0$, $M5ID$, and $CF5C$.

Depending on the test entry, different sizes and numbers of ASME nozzles are used to develop these curve-fits. For example, a test entry with multiple nozzle exit sizes or a nozzle with a variable exit diameter could include a range of available ASME nozzles, from 6 square-inch diameter up to 40 square-inches. If a single customer nozzle size is used, one matching or two bracketing ASME nozzles are typically used to get a better calibration within a smaller range for better accuracy. In general, the more specific the calibration nozzle size and set point conditions are to the customer test article and test matrix, the lower the uncertainty contribution from this calibration. Sensitivities from the $[U]$ matrix, correction coefficient $CFXP0$, and $ALS3$ curve-fit coefficients previously determined from the push-pull, tank pressure, and pressure tare calibrations are fed into the data reduction sequence for the ASME calibration, in addition to several other facility measurements. This data reduction is depicted in Figures 18 and 19. If secondary lines are to be used in the customer test, coefficients from that calibration would be included as well.

5.6 Customer test

All sensitivities and coefficients determined from the calibrations are fed into the data reduction when a customer test is simulated. Data reduction for gross forces and moments are shown in Figures 20 and 21. Further data reduction for several airflow variables of interest are shown in Figure 22.

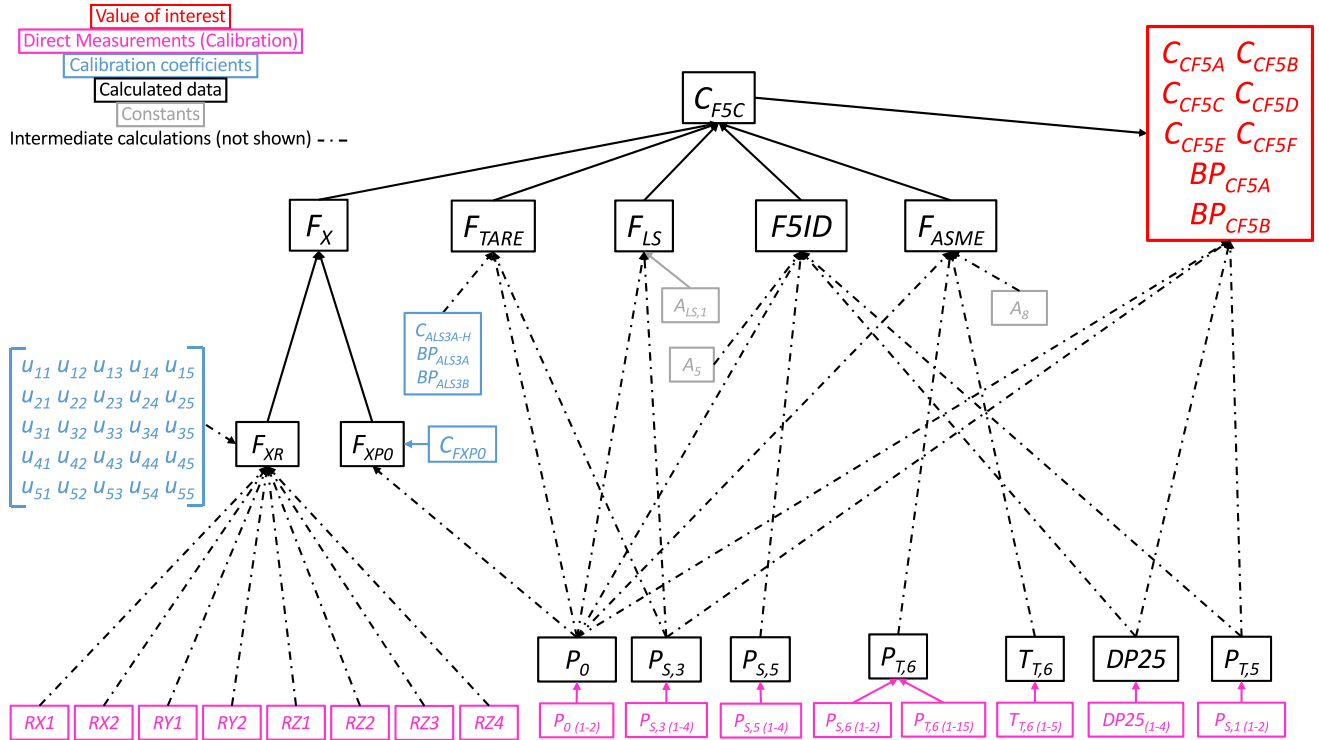


Figure 18: ASME nozzle calibration: Simplified data reduction flow chart for determining CF_5 calibration coefficients

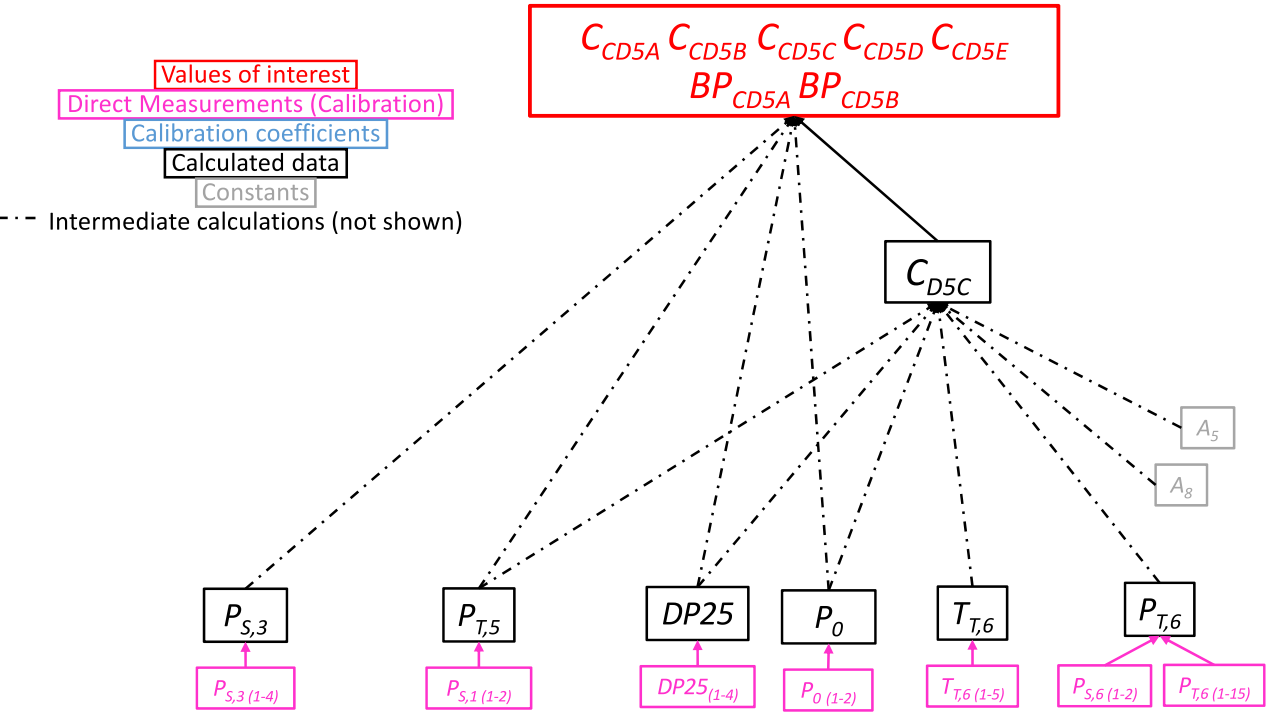


Figure 19: ASME nozzle calibration: Simplified data reduction flow chart for determining CD_5 calibration coefficients

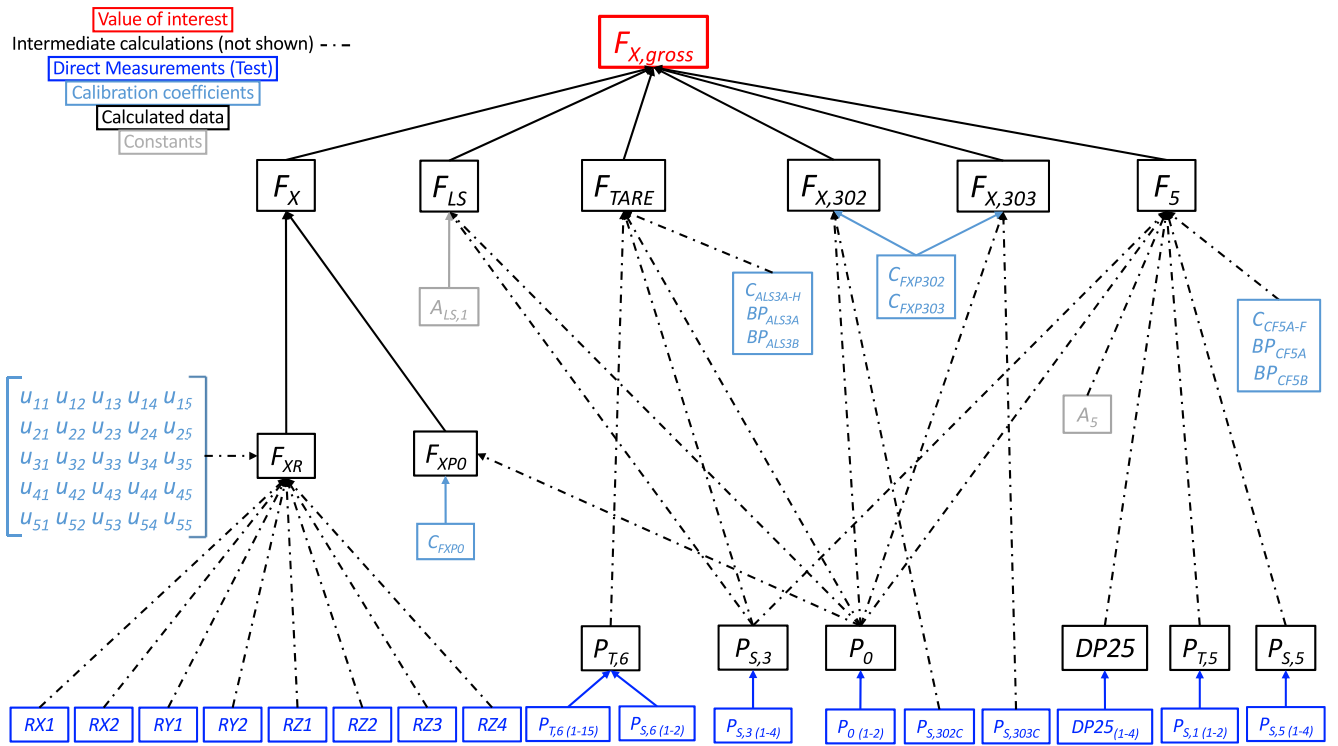


Figure 20: Data reduction flow chart for gross force along the x-axis

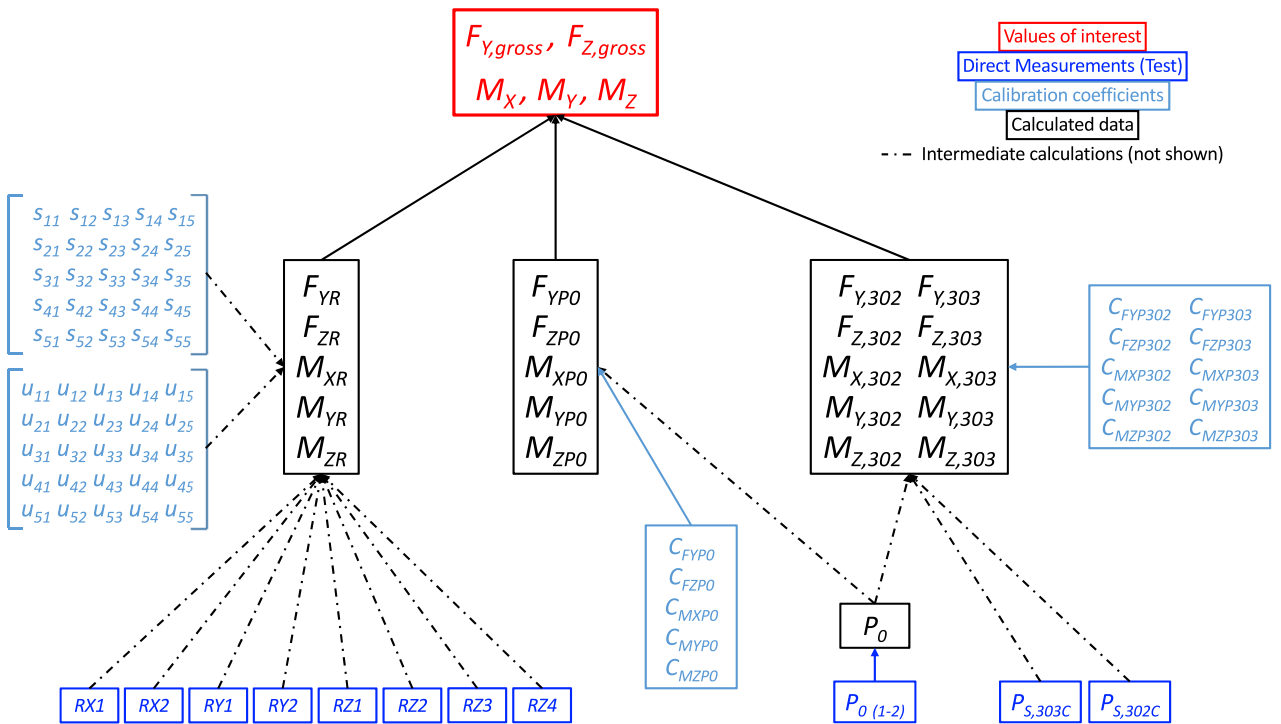


Figure 21: Data reduction flow chart for gross forces along the y- and z-axes and all gross moments

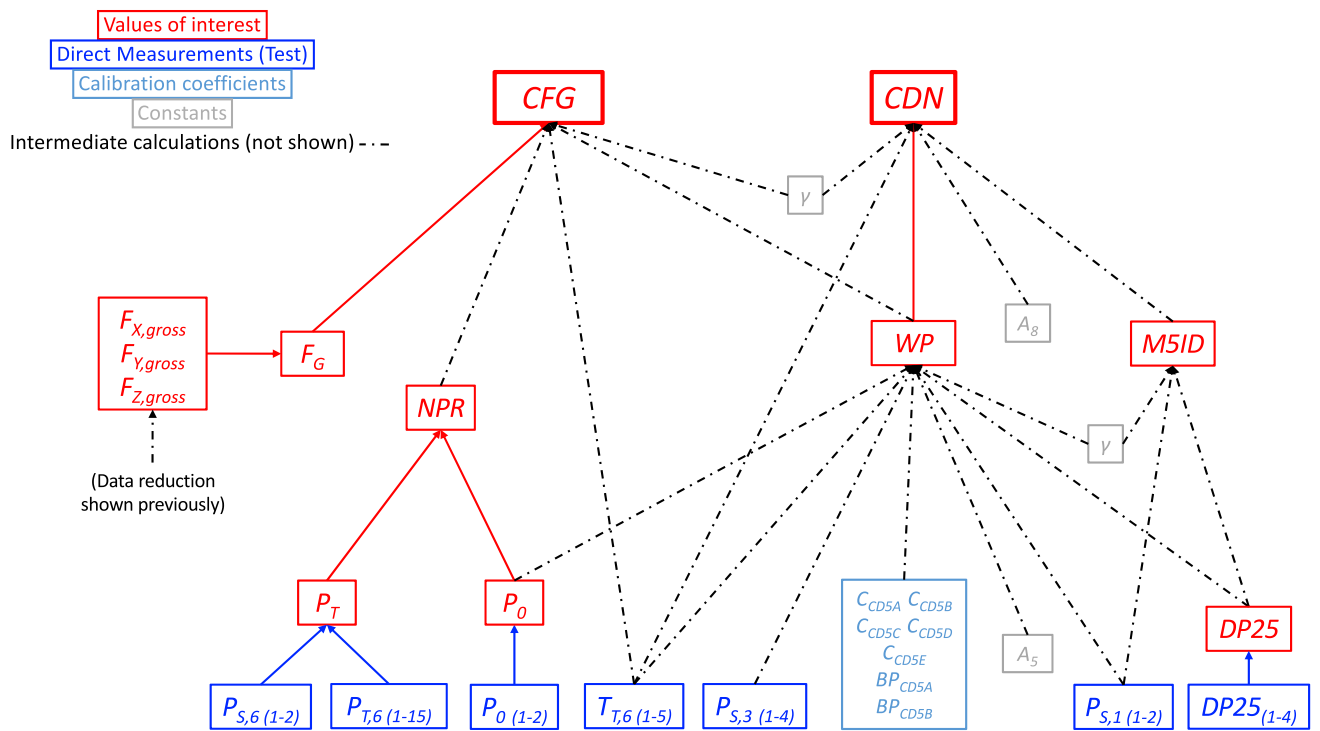


Figure 22: Data reduction flow chart for several airflow variables of interest

6 Uncertainty approach

6.1 General Description

In order to capture systematic uncertainty effects from the calibration sequence referred to in Section 4, an uncertainty propagation approach has been selected to estimate uncertainty in several calculated variables of interest. Short term repeatability of various measurements are also estimated and propagated through to variables of interest to obtain overall uncertainty estimates. (While long term reproducibility is also of interest, data to support this type of estimate is not available at this time.)

The Taylor Series Method (TSM) for uncertainty propagation is employed by MANTUS (“Measurement Analysis Tool for Uncertainty in Systems”) [4], a Microsoft Excel based tool which allows the user to break down the overall measurement into component parts, or “modules”, to easily handle the analysis of multi-level instrumentation systems. This, in essence, captures instrument chain uncertainty contributions from the point of measurement through the data system output as depicted in Figure 23.

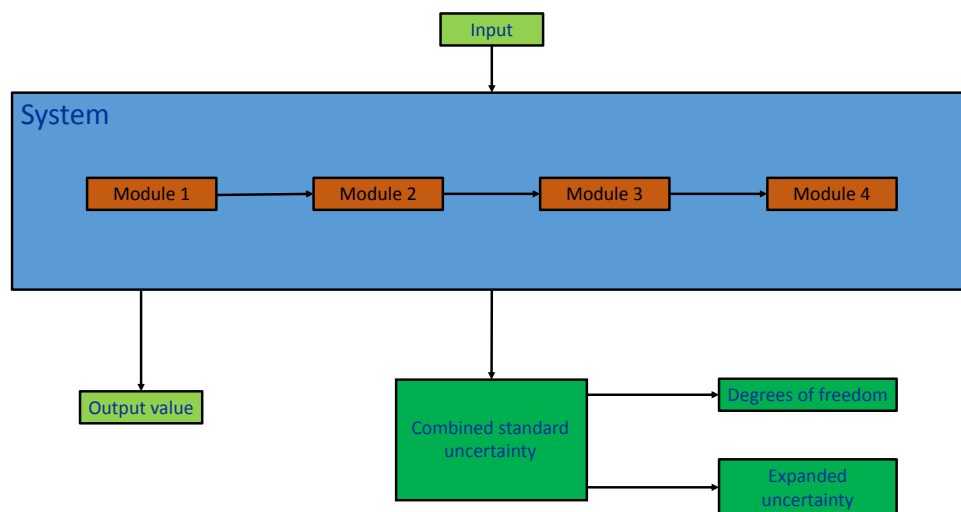


Figure 23: Instrumentation level uncertainty analysis flow

The Monte Carlo Method (MCM) of uncertainty propagation was selected to further propagate random and systematic measurement uncertainties through the data reduction sequences for all calibrations and “test time” simulations listed in Section 5. In brief, the MCM allows one to simulate tens of thousands “synthetic realizations” of a test point, test matrix, or sequence of tests. Using uncertainty estimates, appropriate error populations are produced and added to associated measurements, simulating errors from certain uncertainty sources. This produces large populations of perturbed quantities of all measurements taken during a test. Each set of perturbed measurements is then sent through the entire data reduction sequence to achieve thousands of simulated calculations of variables of interest. The perturbed populations of the variables of interest can then be analyzed to assess measurement uncertainty in each variable.

The MCM was selected in lieu of the TSM due to the large number of calculations involved and several measurement uncertainty correlations present in the data reduction sequence. The method also lends itself well to quickly simulating theoretical changes for investigation of potential uncertainty improvements. For specific details on the methodology and application of both TSM and MCM, including examples of error population for uncorrelated and correlated uncertainties, see references [4] and [5].

6.2 Elemental standard uncertainty estimates

Using concepts from the ISO *Guide to the Expression of Uncertainty in Measurement* [6], Coleman and Steele [5] define an elemental standard uncertainty as "an estimate of the standard deviation of the parent population from which a particular elemental error originates." All elemental standard uncertainty estimates, sources, and quantities which serve as inputs into the error propagation are detailed in this section (standard, 1-sigma uncertainty estimates are presented). Elemental standard uncertainty estimates for measurement x will be denoted as b_x and s_x , following standard nomenclature for systematic standard and random standard uncertainty categorization, respectively. As best as possible, the Monte Carlo simulation implements error population properly based on assumed error distributions, uncertainty correlations between measurements, and uncertainty correlations between test entries (each calibration is considered a separate test entry since they are separated by several days or months). Unless otherwise noted, a normal distribution of errors is assumed for elemental uncertainties propagated. Calibration cycles of all instruments involved in the data reduction are considered and accounted for within the simulations. The specific heat ratio for air, γ , as well as gas constants used in the data reduction scheme are assumed to have negligible uncertainty contributions.

6.2.1 Pressure measurements

Most pressure measurements in CE22 are obtained by ± 15 psid, 45psid, and 500psid range pressure units within the S3200 Electronic Scanning Pressure (ESP) system. All pressures which share a common pressure calibration unit (PCU) are calibrated to the same reference pressure, and are therefore considered to have fully correlated systematic errors for measurements obtained within a calibration cycle. A barometric pressure, P_{bar} , is also measured by the ESP system which contains systematic uncertainty; the random uncertainty of the barometric pressure unit is considered negligible. Standard uncertainty estimates associated with ESP are listed in Table 4.

Uncertainty Label		Standard Uncertainty Estimate	Source of Estimate
$b_{P_{bar}}$		0.00214 psi	MANTUS
$b_{P,ESP15}$		See Figure 24	MANTUS
$s_{P,ESP15}$	Airflow off ^d	0.00054 psi	Short term variability observed[1]
	Airflow on	0.00067 psi	
$b_{P,ESP45}$		See Figure 25	MANTUS
$s_{P,ESP45}$	Airflow off	0.0039 psi	Short term variability observed[1]
	Airflow on	0.013 psi	
$b_{P,ESP500}$		See Figure 26	MANTUS
$s_{P,ESP500}$	Airflow off	0.00095 psi	Short term variability observed[1]
	Airflow on	0.0032 psi	

Table 4: Elemental uncertainty estimates for ESP pressure measurements

^dSome of the calibrations are performed with facility airflow off, such as the Push-Pull and Tank Pressure calibrations. Variability of measurements changes with airflow on/off conditions.

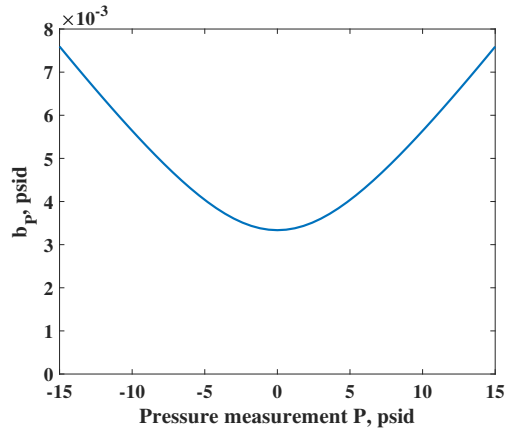


Figure 24: Systematic standard uncertainty estimate for ± 15 psid ESP system

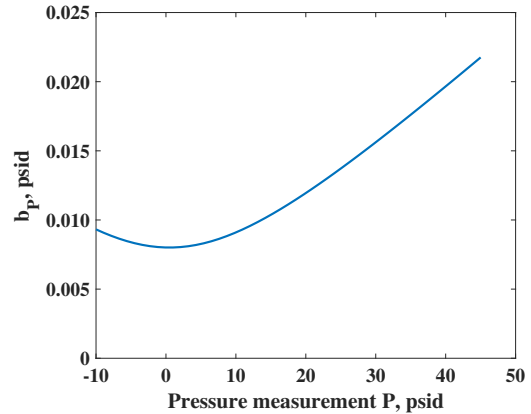


Figure 25: Systematic standard uncertainty estimate for 45psid ESP system

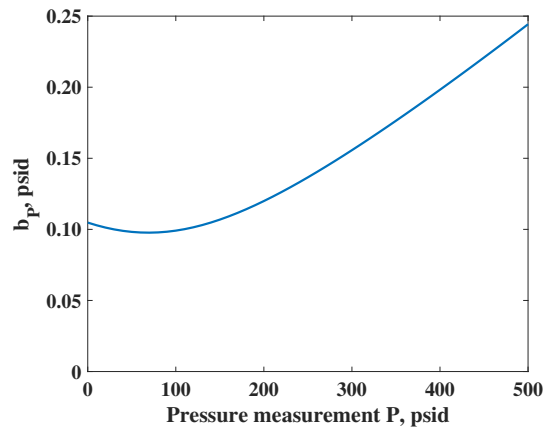


Figure 26: Systematic standard uncertainty estimate for 500psid ESP system

There are additionally a set of 1psid, 2psid or 5psid differential pressure transducers installed to measure the delta pressure between stations 2 and 5 (DP_{25}). Based on the required set points of the test entry, the minimum DP range that can be used to satisfy all test conditions without risking over-ranging the transducers is installed. Systematic uncertainties are shown for all DP ranges in Table 5. A correlated and uncorrelated portion of uncertainty is shown for each transducer range; the correlated portion of uncertainty is propagated as a common error experienced by all measurements from these instruments, arising from use of a common signal conditioner. Since each transducer is calibrated separately, each also carries an uncorrelated portion of uncertainty. For this analysis, the 5psid DP uncertainty is propagated to provide the most conservative estimate of overall uncertainty in selected variables of interest.

6.2.2 Temperature measurements

Temperature measurements in CE-22 are obtained using bi-metal Type K thermocouples connected to a reference oven. Like the DP transducers, the thermocouples have both uncorrelated and correlated uncertainty components; the correlated portion results from the shared reference oven. Standard uncertainty estimates for temperature measurements are shown in Table 6.

Uncertainty Label and Description			Standard Uncertainty Estimate	Source of Estimate
b_{DP25}	1psid	Uncorrelated	0.00095 psi	MANTUS
		Correlated	0.0003 psi	
	2psid	Uncorrelated	0.0020 psi	
		Correlated	0.00075 psi	
	5psid	Uncorrelated	0.0085 psi	
		Correlated	0.0015 psi	
s_{DP25}	(All DP ranges)	Airflow off	0.00054 psi	Short term variability observed[1]
		Airflow on	0.00067 psi	

Table 5: Elemental uncertainty estimates for differential pressure measurements ($DP25$)

Uncertainty Label and Description		Standard Uncertainty Estimate	Source of Estimate
b_{TT}	Uncorrelated	2.8°R	MANTUS
	Correlated	0.45°R	
s_{TT}		0.25°R	Short term variability observed[1]

Table 6: Elemental uncertainty estimates for thermocouple measurements (TT)

6.2.3 Force measurements

The thrust stand uses both $\pm 2,000$ lbf and $\pm 4,000$ lbf load cells. While MANTUS quantifies uncertainties associated with these instrument measurement systems, the Push-Pull calibration has an extensive test matrix, providing well-characterized information of the thrust stand behavior as a unit [3]. This is valuable data since mechanical assemblies have inherent hysteresis and non-linearity characteristics, carrying uncertainties that would be neglected if only the elemental uncertainties of the load cell measurements are directly propagated. Therefore, instead of propagating the systematic standard uncertainty of each individual load cell, data from the Push-Pull calibration is used to estimate a systematic standard uncertainty for each combination of reaction loads that was used to develop the thrust stand sensitivities.

Figure 27 shows an example of data obtained from one loading sequence from the Push-Pull calibration test matrix. This particular data set shows the combination of reaction loads $RZ1 + RZ2$ to the applied calibration load $FY_{applied} = CY1 + CY2$ (see Figure 7 for load cell locations). The standard uncertainty estimate for the combination of reaction loads is obtained by evaluating the standard error of the estimate, s_{yx} , using residuals from the linear least squares fit with Equation 1

$$s_{yx} = \sqrt{\frac{\sum_{i=1}^k (y_i - \hat{y}_i)^2}{v_{s_{yx}}}} \quad (1)$$

where k is the number of (x_i, y_i) data pairs used to create the curve-fit, v represents the degrees of freedom in s_{yx} (for polynomials of fit order m , $v_{s_{yx}} = k - (m + 1)$), and \hat{y}_i is the predicted value at x_i [7]. This standard uncertainty estimate is essentially the standard deviation of the residuals from the fit, and propagating this standard uncertainty captures the variation in the force result predicted by the curve-fit. Uncertainty associated with the prediction of thrust stand forces as their combined effect is denoted $b_{PPs_{yx}}$ within this document.

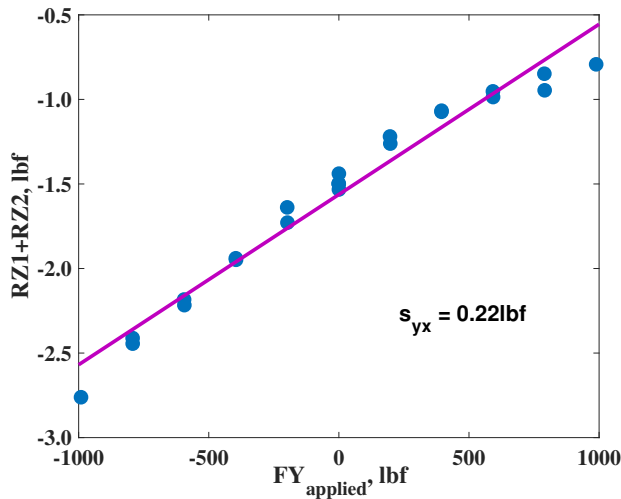


Figure 27: Example of thrust stand force uncertainty determination for $b_{\mu_{4,2}}$ (see Figure 10)

Since all loads are tared before a loading sequence begins during calibration and testing, the zero offset components (by far the largest contributor) of uncertainty in load cell measurements are mitigated and therefore considered negligible. The systematic standard uncertainty estimates for all combinations of loads determined during the Push-Pull calibration are summarized in Tables 7 and 8, presented in matrix form corresponding to $[\mathbf{S}]^{-1}$ and $[\mathbf{U}]^{-1}$ matrices (Figures 9 and 10).^e Uncertainty in the slopes themselves are determined through propagation of uncertainties using the MCM through data reduction of the entire Push-pull calibration and are fossilized within each MC iteration.

$b_{\sigma_{i/j}}$	1	2	3	4	5
1	0.42	0.31	0.58	0.06in ⁻¹	0.03in ⁻¹
2	0.25	0.43	0.83	0.09in ⁻¹	0.04in ⁻¹
3	0.59	0.64	1.98	0.18in ⁻¹	0.06in ⁻¹
4	0.16	0.71	2.17	0.27in ⁻¹	0.05in ⁻¹
5	0.40	0.52	1.31	0.12in ⁻¹	0.04in ⁻¹

Table 7: Systematic standard uncertainty estimates for load combinations corresponding to the $[\mathbf{S}]^{-1}$ matrix

$b_{\mu_{i/j}}$	1	2	3	4	5
1	0.42	0.31	0.58	0.03in ⁻¹	0.03in ⁻¹
2	0.25	0.43	0.83	0.04in ⁻¹	0.04in ⁻¹
3	0.58	0.64	1.98	0.09in ⁻¹	0.06in ⁻¹
4	0.10	0.22	0.82	0.04in ⁻¹	0.02in ⁻¹
5	0.40	0.35	2.12	0.11in ⁻¹	0.02in ⁻¹

Table 8: Systematic standard uncertainty estimates for load combinations corresponding to the $[\mathbf{U}]^{-1}$ matrix

The random standard uncertainty estimates for the force measurements are made using observed short term variability. For the state of the facility with airflow off, the random standard uncertainty estimate is $s_F = 0.06\text{lbf}$;

^eFor components of the matrix that required use of multiple fits to deduce the sensitivity, the standard errors of the two fits were root-sum-squared to acquire the combined effect of the standard error (the last two columns in both the $[\mathbf{S}]^{-1}$ and $[\mathbf{U}]^{-1}$ matrices). Also, division by thrust stand lengths were included in the sensitivity calculation where necessary to obtain the proper uncertainty.

for airflow on conditions, the estimate is $s_F = 1.58\text{ lbf [1]}$.^f The airflow on condition variability is presumed to be higher due to the dynamic response of the thrust stand to the airflow.

6.2.4 Lengths and Areas

Other elemental uncertainty estimates that are propagated in this analysis include systematic uncertainties from distance measurements on the thrust stand (used primarily in the data reduction to calculate moments about the X-, Y-, and Z-axes) and on diameters of facility ducts and test articles (used to determine critical areas which directly impact airflow related calculations). Table 9 shows the systematic standard uncertainty estimates propagated in the analysis and the sources of the estimates. Random uncertainty is assumed to be negligible for all of these measurements.^g

Uncertainty Label and Description		Standard Uncertainty Estimate	Source of Estimate
b_L		0.005in	Facility prints
b_{A5} ^h		0.067in ²	
b_{ALS1} ⁱ		0.234in ²	
$b_{A8,ASME}$	6in ² nozzle	0.0012in ²	Calibration lab
	15in ² nozzle	0.0019in ²	
	24in ² nozzle	0.0024in ²	
	30in ² nozzle	0.0027in ²	
	40in ² nozzle	0.0031in ²	

Table 9: Elemental systematic standard uncertainty estimates for lengths and areas

6.2.5 Regression Uncertainty

There are two aspects of uncertainty that need to be considered when dealing with regressions as part of the data reduction scheme. The first is the uncertainty that is fossilized within the calibration curve itself, which results from errors (random and systematic) that are present within the data set used to form the regression in the first place. These errors impact the regression curve in a systematic nature and are categorized as such. A Monte Carlo simulation of the calibration test through production of the regression equation, including propagation of all uncertainties involved, captures the uncertainty of the regression curve itself and represents how much the entire curve-fit varies due to uncertainties present during the calibration test. (This is synonymous with the confidence interval of the regression fit. The TSM of this aspect of regression uncertainty is presented in Reference [5].)

The second aspect to be considered is the ability of the regression to predict a future value. This aspect of the estimate considers how well the data is characterized by the calibration curve, and provides an estimate of the uncertainty in the value predicted by the fit. This includes amount of random variability around the fit and goodness-of-fit of the regression. By analyzing residuals, uncertainty estimates can be made to capture this aspect of uncertainty which is applied to a variable each time the curve is used to predict its value. When analyzing residuals of a regression fit, it is typically fairly obvious by visual inspection whether the residuals are random in nature (this can also be confirmed by statistical analysis) or if they are more systematic in nature (for example, if the actual response is a second-order behavior yet a first-order fit was selected). This distinction impacts uncertainty categorization and the nature of the error distribution; the important thing to note is that propagation through

^fUncertainty estimates made from random variation observations noted in reference [1] are deduced from ten back-to-back samples taken at 1Hz. These are short term observations and are not expected to capture long term variation. Standard deviations reported in the noted reference are divided by the square root of ten to reflect the expected variation of the mean of ten samples used to represent a steady state data point. $\sigma_{\bar{x}} = \sigma_x / \sqrt{10}$

^gThese uncertainty estimates are based on drawing specifications and calibration lab quotes; it is assumed the quality control of the measurements used to confirm specifications were repeatable to a negligible level.

^hUncertainties in A5 and A8 are displayed in this chart as "elemental" uncertainties but were in fact propagated from uncertainty in the diameters.

ⁱWhile the standard uncertainty in ALS1 is quoted here and formally propagated, the error term cancels out when data reduction is followed, resulting in no impact on any uncertainties of interest.

the regression alone will not inherently account for this second aspect of regression uncertainty. This uncertainty must be explicitly evaluated and propagated. This "uncertainty in the prediction" is needed in addition to the fossilized uncertainty of the regression curve itself for proper evaluation of uncertainty of a future single data point predicted by the curve.

Elemental measurement uncertainties were propagated via Monte Carlo for each calibration test performed in CE-22 to develop the confidence interval for all curve-fits determined. Uncertainty estimates for the predictive quality of each regression fit were also made. For the Tank Pressure and Secondary Line calibrations, Equation 1 was used for each calibration curve developed to obtain an uncertainty estimate for the value predicted by the linear fit, the combined uncertainty from each denoted by s_{P0syx} and s_{SECsyx} . These standard uncertainty estimates can be found in Tables 10 and 11, and are categorized as random uncertainties.

Uncertainty label	Standard uncertainty estimate
s_{FXP0}	1.0 lbf
s_{FYP0}	0.6 lbf
s_{FZP0}	2.2 lbf
s_{MXP0}	23.3 lbf-in
s_{MYP0}	2.9 lbf-in
s_{MZP0}	5.2 lbf-in

Table 10: Uncertainties associated with predicting values from Tank Pressure ($P0$) linear calibration fits

Uncertainty label	Standard uncertainty estimate
s_{FXP302}	0.2 lbf
s_{FYP302}	0.3 lbf
s_{FZP302}	0.2 lbf
s_{MXP302}	3.7 lbf-in
s_{MYP302}	3.1 lbf-in
s_{MZP302}	4.6 lbf-in
s_{FXP303}	0.2 lbf
s_{FYP303}	0.1 lbf
s_{FZP303}	0.7 lbf
s_{MXP303}	11.8 lbf-in
s_{MYP303}	22.1 lbf-in
s_{MZP303}	2.6 lbf-in

Table 11: Uncertainties associated with predicting values from Secondary Line linear calibration fits

For the ALS3 (Pressure Tare) and ASME calibrations, the residuals were studied and representative uncertainty bands selected to estimate appropriate standard uncertainty intervals, denoted $s_{ALS3syx}$ and $b_{ASMEsyx}$. This method was selected in lieu of using Equation 1 because variability was not constant along the range of these particular fits. The standard and expanded uncertainty estimates for the regression performed for the ALS3 correction is shown in Figure 28; the standard uncertainty estimate is categorized as random, and is defined by

$$s_{ALS3syx} = \frac{0.5}{PS3QP0} [\text{in}^2] \quad (2)$$

where $PS3QP0$ is the pressure ratio of $PS3/P0$. An example of an error population that was created using this estimate for a single Monte Carlo iteration of the ALS3 test simulation is shown in Figure 29. The simulated error population compares favorably to the actual fit errors.

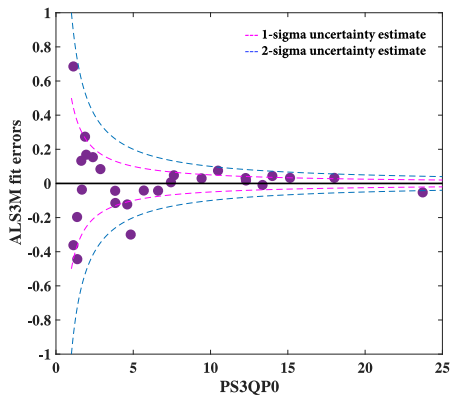


Figure 28: ALS3 calibration/correction residuals and $s_{ALS3syx}$ uncertainty estimate

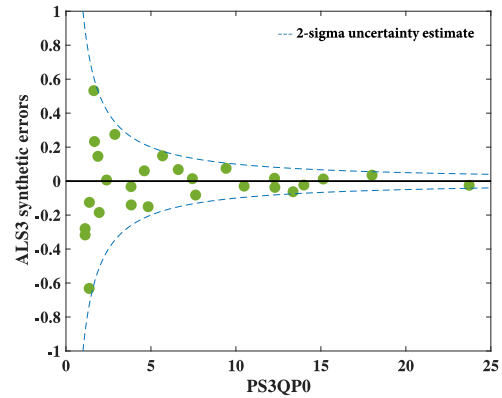


Figure 29: Example of synthetic error population produced by $s_{ALS3syx}$ from a single MC iteration when fit is used to predict ALS3 values

The standard and expanded uncertainty estimates for predictions of $CD5$ and $CF5$ from the ASME calibration are driven by the specific calibration performed pre-customer test. Due to the large variety of possible nozzle sizes and test conditions within individual test programs (along with the facility standard procedure to cater the ASME calibration accordingly), results for uncertainty estimates from this calibration are not generalized in this report. An example is presented in Section 7.5 showing results that can be generated post-ASME calibration. Note that estimates given in the example for this uncertainty source are not to be generalized, as they vary widely based on the specific calibration and test conditions.

6.3 Summary of uncertainty inputs

As a detailed uncertainty analysis is updated and refined, it is important to have a handle on what uncertainties have been estimated and propagated so that updates and changes can easily be made. Table 12 summarizes the uncertainties (detailed previously in this chapter) that were propagated and the nomenclature associated with the estimates within this report so that in the results section, these uncertainty sources can be identified. Many uncertainties of specific measurements and variables were grouped in the propagation code in order to expedite run time.

Uncertainty label	Description	Variables to which uncertainty is applied
$s_{P,ESP15}, b_{P,ESP15}$	Random, systematic uncertainty of 15-psid ESP measurements	$P0$
$s_{P,ESP45}, b_{P,ESP45}$	Random, systematic uncertainty of 45-psid ESP measurements	$PT6, P51-6$
$s_{P,ESP500}, b_{P,ESP500}$	Random, systematic uncertainty of 500-psid ESP measurements	$P5302C, P5303C$
s_{DP25}, b_{DP25}	Random, systematic uncertainty of differential pressure measurements	$DP25$
s_{TT}, b_{TT}	Random, systematic uncertainty of total temperature measurements	$TT6$
s_F	Random uncertainty of load cell measurements	$RX1-2, RY1-2, RZ1-4, CX1-2, CY1-2, CZ1-4$
b_{Pbar}	Systematic uncertainty of barometric pressure within ESP system	All ESP measured pressures
b_{ALS1}	Systematic uncertainty associated with area measurement $ALS1$	$ALS1$
b_{A5}	Systematic uncertainty associated with area measurement $A5$	$A5$
b_{A8NOZZ}	Systematic uncertainty associated with nozzle exit area $A8$	$A8$
b_{PPsyx}	Systematic uncertainty associated with prediction of corrected thrust stand forces	$FXR, FYR, FZR, MXR, MYR, MZR$
s_{P0syx}	Random uncertainty associated with prediction of tank pressure corrections	$FXP0, FYP0, FZP0, MXP0, MYP0, MZP0$
s_{SECSyx}	Random uncertainty associated with prediction of secondary line corrections	$FXP302, FXP303, FYP302, FYP303, FZP302, FZP303, MXP302, MXP303, MYP302, MYP303, MZP302, MZP303$
$s_{ALS3syx}$	Random uncertainty associated with prediction of frictional force through labyrinth seal	$ALS3$
$b_{ASMEsyx}$	Systematic uncertainty associated with prediction of thrust and flow coefficients	$CD5, CF5$
b_{PPCAL}	Systematic uncertainty associated with propagation of all uncertainties, systematic and random, within the Push-Pull calibration	Fossilized within $[S]$ and $[U]$ matrices
b_{POCAL}	Systematic uncertainty associated with propagation of all uncertainties, systematic and random, within the Tank Pressure calibration	Fossilized within Tank Pressure calibration coefficients
b_{SECCAL}	Systematic uncertainty associated with propagation of all uncertainties, systematic and random, within the Secondary Line calibration	Fossilized within Secondary Line calibration coefficients
$b_{ALS3CAL}$	Systematic uncertainty associated with propagation of all uncertainties, systematic and random, within the $ALS3$ or Pressure Tare calibration	Fossilized within $ALS3$ calibration coefficients
$b_{ASMECAL}$	Systematic uncertainty associated with propagation of all uncertainties, systematic and random, within the $ASME$ calibration	Fossilized within $CD5$ and $CF5$ calibration coefficients

Table 12: Summary of inputs to uncertainty propagation

7 Results

Depending on the test being performed, researchers and customers are often interested in different aspects of uncertainty. For example, customers refining a design element by comparing multiple test entry results with one another are primarily concerned with random uncertainty (or repeatability) and its effect on the results, whereas a systematic bias may be less consequential to the study at hand. However, customers seeking to confirm a CFD model with test results may be very concerned with systematic uncertainty effects. For this reason, combined (overall, all inclusive) uncertainty results are presented by variable of interest, and are also broken down into their random and systematic components. Further breakdowns by uncertainty percent contribution (UPC) are performed for the random uncertainty results for each variable of interest.^j

Uncertainty results are produced by running a system of Monte Carlo simulations of the entire calibration sequence in addition to a "test-time" simulation, representative of a customer test. Uncertainty results covering a majority of the facility's range^k will be presented in this section with the exception of the following variables: *WP*, *FXG*, *FG*, *CFG* and *CDN*. Calculations of these variables occur "downstream" of the ASME calibration, to which they are highly sensitive. For these listed variables, example results are shown in Section 7.5 for one specific ASME calibration and customer test sequence. It is standard facility practice to provide a specific calibration for each test entry, catered to match or bracket conditions designed for that customer's test. Because they are so very specific, uncertainty results for these variables should not be extrapolated or assumed to apply to all facility conditions or nozzle sizes. Uncertainty estimates for these critical variables will be made available to customers once the ASME calibration that is specifically catered to their test is complete. Pre-test entry estimates can be provided upon request if data and information are available to support the request.

All uncertainty results are presented as expanded uncertainties, denoted by S_x , B_x , and U_x for random, systematic, and combined uncertainty respectively, and are presented with a 95% level of confidence.

7.1 *P0*, *PT*, *DP25*, *NPR*: Critical facility calculations

7.1.1 Random Uncertainty

Critical facility pressure calculations have expanded random uncertainties presented in Table 13. Propagated estimates for variation in the 5-psid Sensotec differential measurements, 15-psid ESP measurements, and 45-psid ESP measurements are the sole contributors to uncertainty in calculated values for *DP25*, *P0* and *PT*, respectively. Figure 30 shows the dimensional expanded random uncertainty estimate for *NPR* (*PT* = 45psia) and the UPC of contributing uncertainty sources to *NPR*.

Variable x	Random uncertainty, S_x , psi
<i>DP25</i>	8.0×10^{-4}
<i>P0</i>	9.4×10^{-4}
<i>PT</i>	7.2×10^{-3}

Table 13: Expanded random uncertainty in critical facility pressures *P0*, *PT*, and *DP25*

^jUncertainty percent contribution for systematic uncertainty results are unable to be obtained for this analysis due to some non-Gaussian distributions of results of individually propagated uncertainty sources. These non-Gaussian distributions were brought about by the data reduction sequence; when all systematic sources are propagated together, a near-Gaussian distribution is achieved so an appropriate symmetric uncertainty quote and coverage factor can be used.

^kLower altitude conditions (below 40psia) were not included in this analysis.

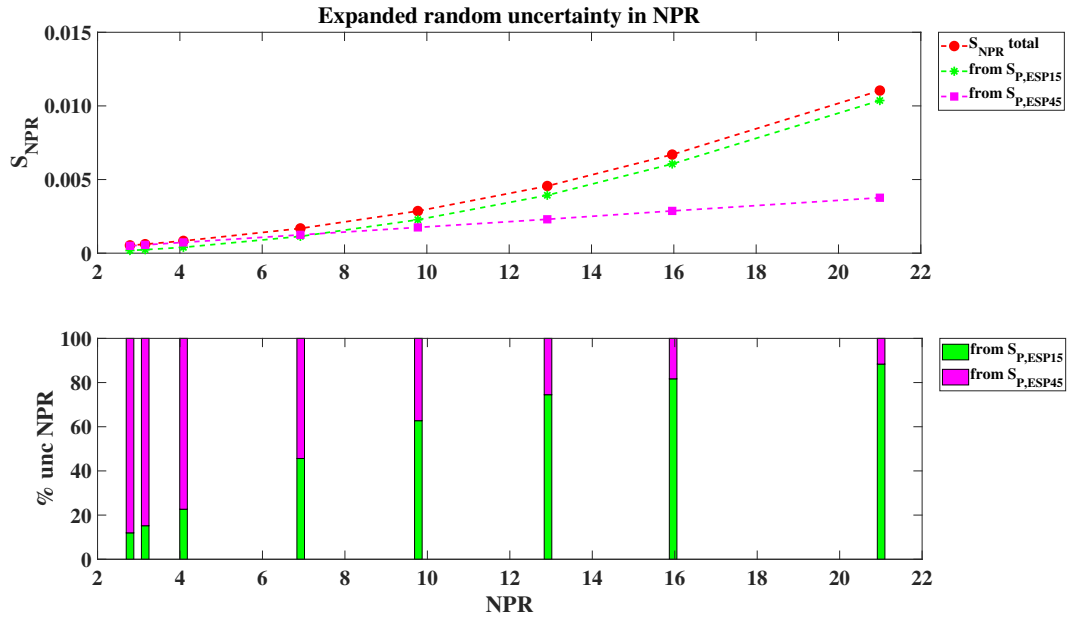


Figure 30: Expanded random uncertainty and UPC contributing to S_{NPR} for $PT = 45\text{psia}$

7.1.2 Systematic and Combined uncertainty

Figure 31 shows the combined, random, and systematic uncertainty for calculated values $DP25$, $P0$, PT , and NPR . Note that the systematic portion of uncertainty greatly drives the combined uncertainty, as they lie on top of each other in several figures. Figure 32 shows how the uncertainty in NPR changes with the total pressure.

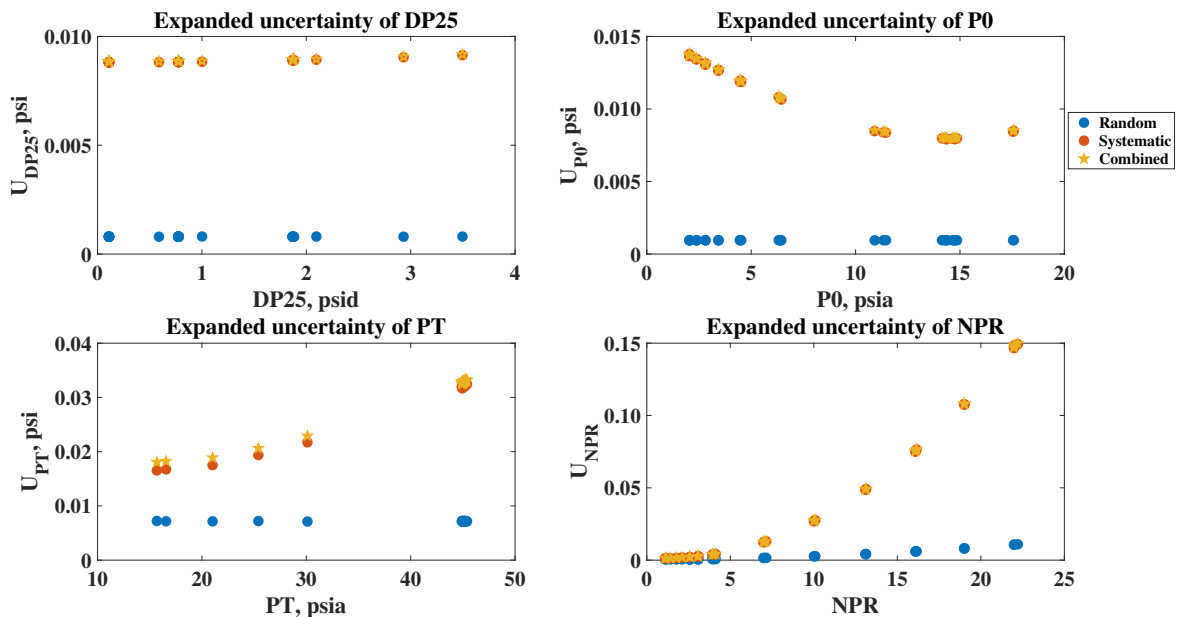


Figure 31: Expanded combined uncertainty for $P0$, PT , $DP25$, and NPR (U_{NPR} shown for $PT = 45\text{psia}$)

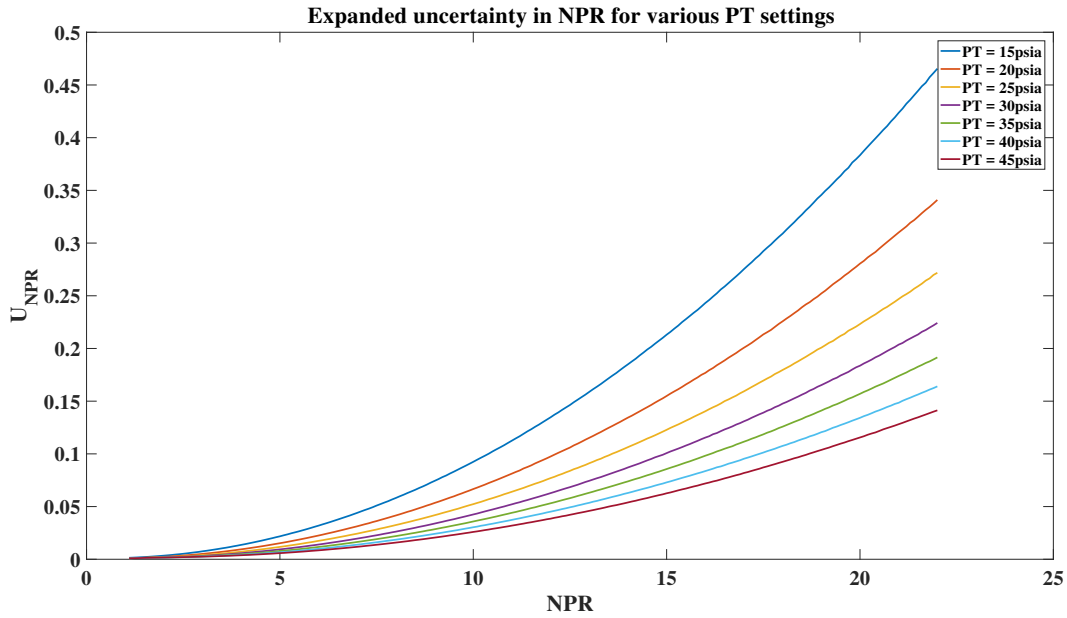


Figure 32: Expanded combined uncertainty in NPR for various PT settings

7.2 $M5ID$: Ideal Mach number at station 5

7.2.1 Random uncertainty

Table 14 shows the expanded random uncertainty of $M5ID$ (ideal Mach number at station 5) for nozzle areas 6-24in² and Figure 33 shows the UPC of contributing elemental random uncertainties for each. Figure 34 shows dimensional random uncertainty contributions as well as the UPC for the 40in² nozzle.

Nozzle area A_8 , in ²	S_{M5ID}
6	2.2×10^{-4}
15	8.4×10^{-5}
24	6.9×10^{-5}

Table 14: Expanded random uncertainty in $M5ID$ for various nozzle sizes (estimates valid across all NPR)

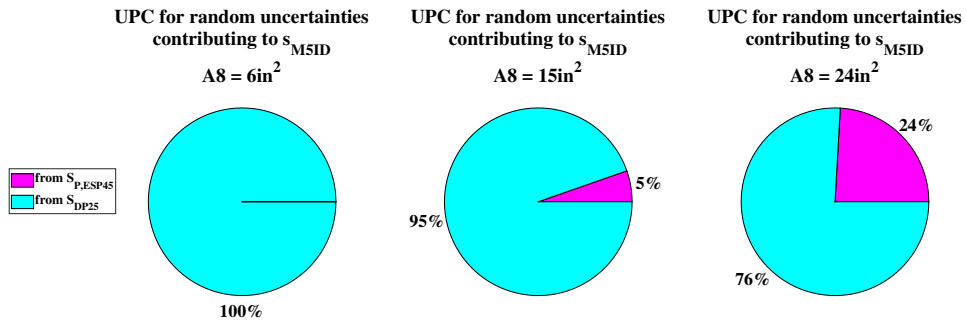


Figure 33: Random UPC contributing to S_{M5ID} for various nozzle sizes

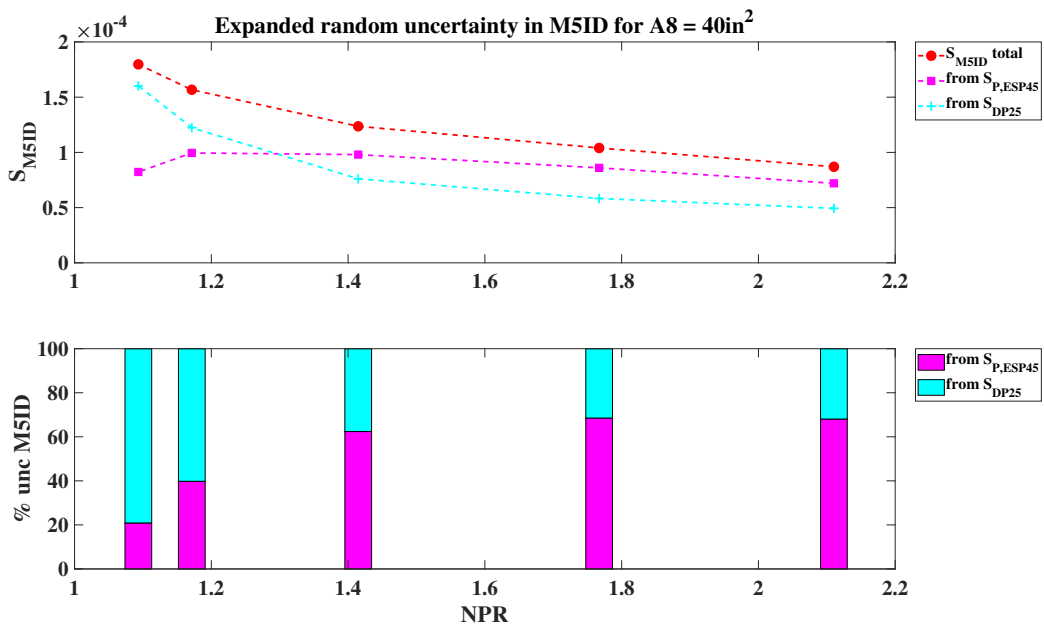


Figure 34: Expanded random uncertainty and UPC contributing to S_{M5ID} for 40in^2 nozzle

7.2.2 Systematic uncertainty

Expanded systematic uncertainty results for $M5ID$ for several simulated nozzle exit areas are shown in Figure 35.

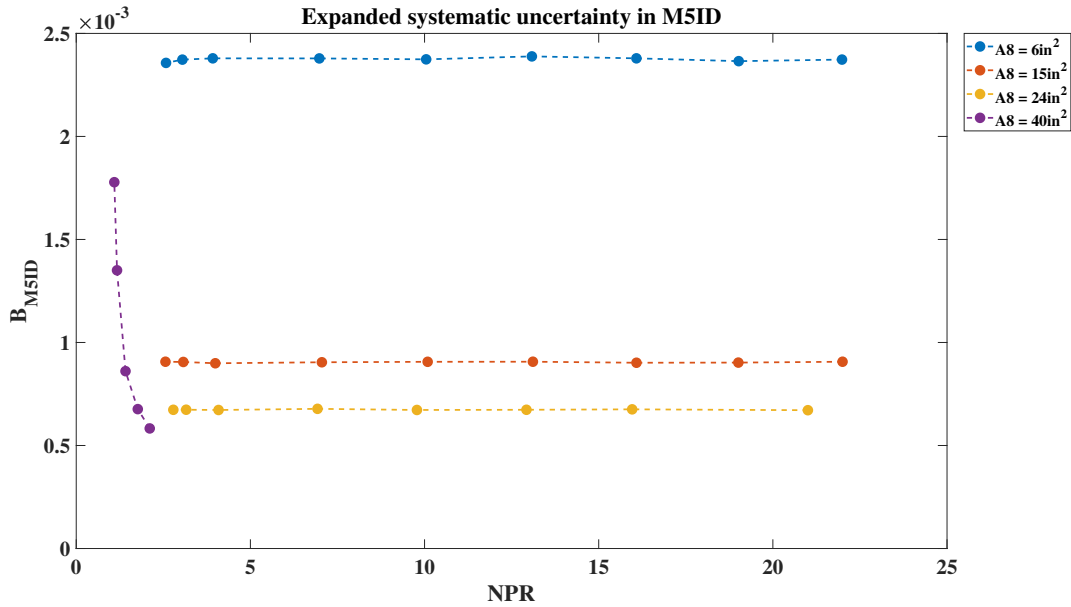


Figure 35: Expanded systematic uncertainty, B_{M5ID} , for various nozzle sizes

7.2.3 Combined uncertainty

Random, systematic, and combined expanded uncertainties for $M5ID$ are displayed in Figure 36 for all nozzle exit areas considered in the test simulation. Note that the systematic component of uncertainty is so dominant, it is effectively equal to the combined uncertainty in these cases.

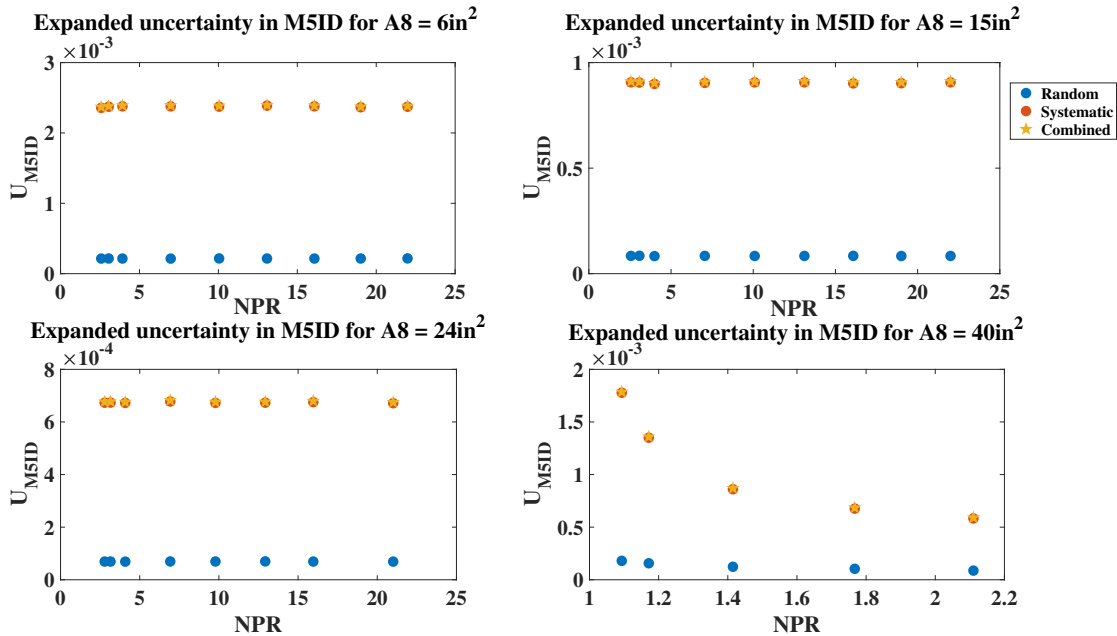


Figure 36: Expanded combined uncertainty, U_{M5ID} , for various nozzle sizes

7.3 FGY, FGZ, MX, MY, MZ: Gross forces and moments

7.3.1 Random uncertainty

Expanded random uncertainty results for directional gross (corrected) forces and moments are shown in Table 15. The associated UPCs are shown in Figure 37, displaying the elemental random uncertainties that influenced total random uncertainty in these variables.

Axis	S_{FG} , lbf	S_M , lbf-in
X	–	88
Y	5.0	147
Z	7.7	81

Table 15: Expanded random uncertainty in gross forces and moments

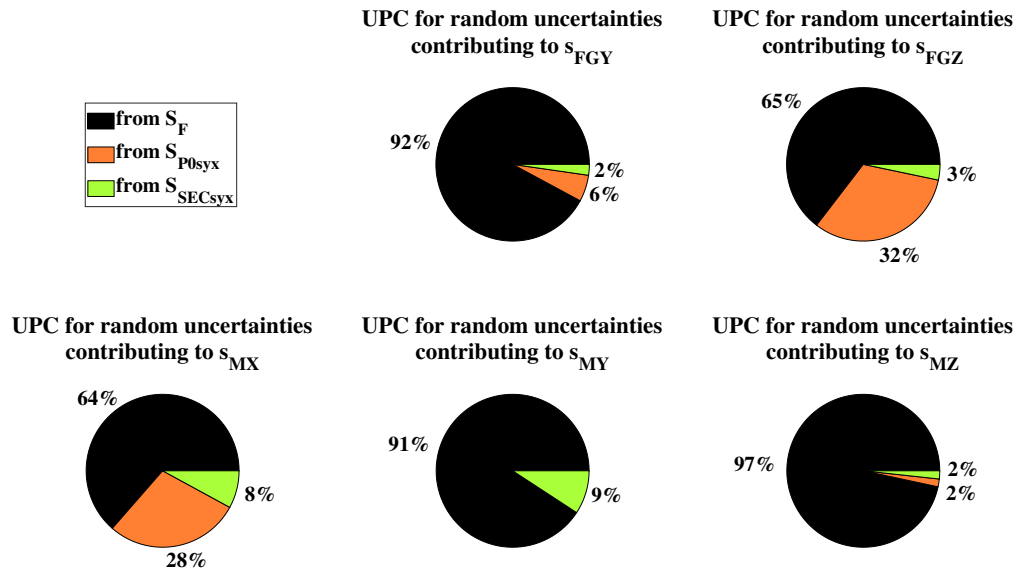


Figure 37: UPC to random uncertainties in gross forces and moments

7.3.2 Systematic uncertainty

Expanded systematic uncertainty results for gross forces, FGY and FGZ , and moments are shown in Figures 38 and 39, respectively.

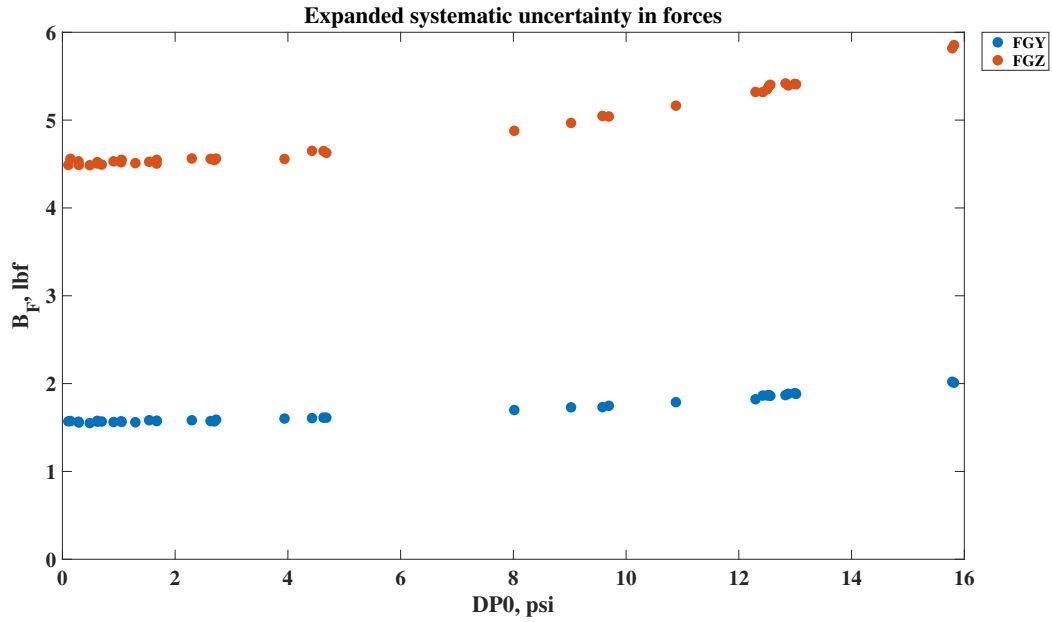


Figure 38: Expanded systematic uncertainty in directional gross forces FGY and FGZ

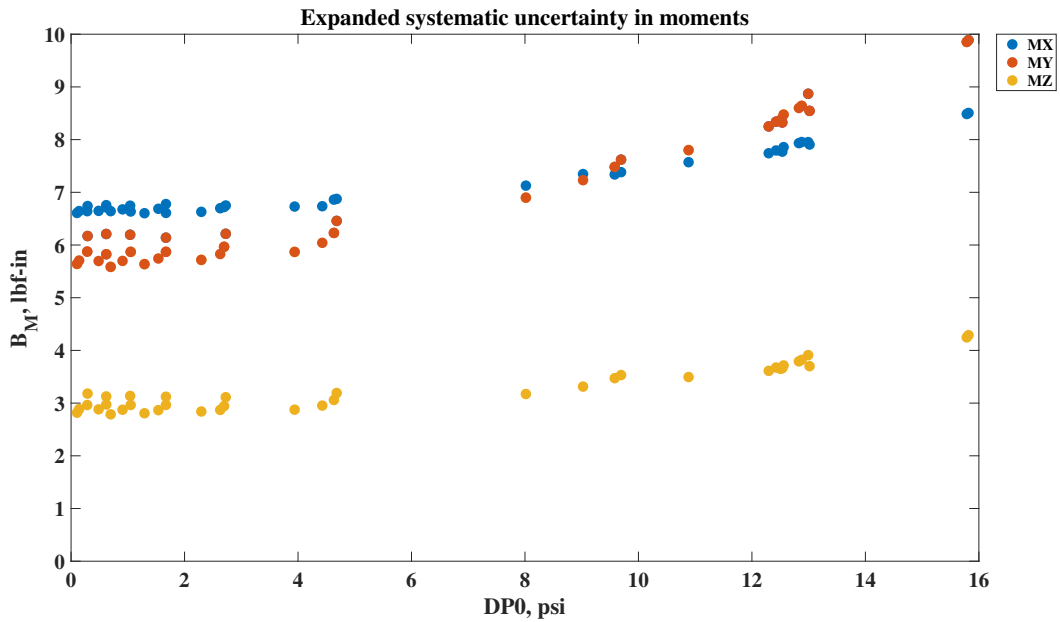


Figure 39: Expanded systematic uncertainty in moments

7.3.3 Combined uncertainty

Random, systematic, and combined expanded uncertainties for gross forces, FGY and FGZ , and moments are shown in Figures 40 and 41, respectively. Note that for moments, the random component of uncertainty is so dominant, it is effectively equal to the combined uncertainty for these variables.

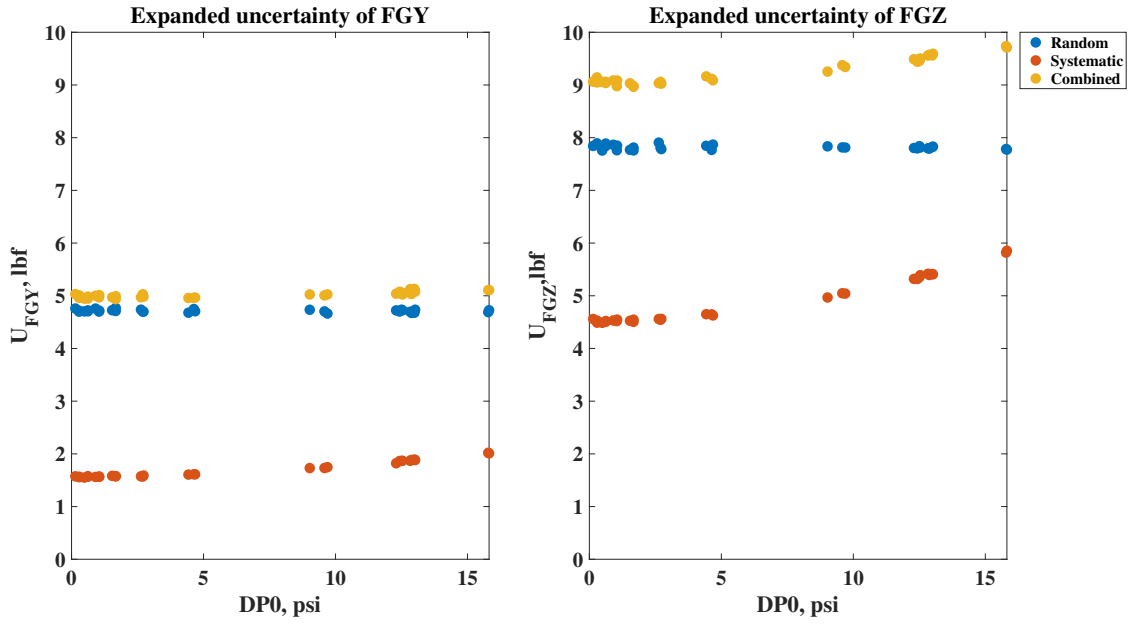


Figure 40: Expanded combined uncertainty in gross forces FGY and FGZ

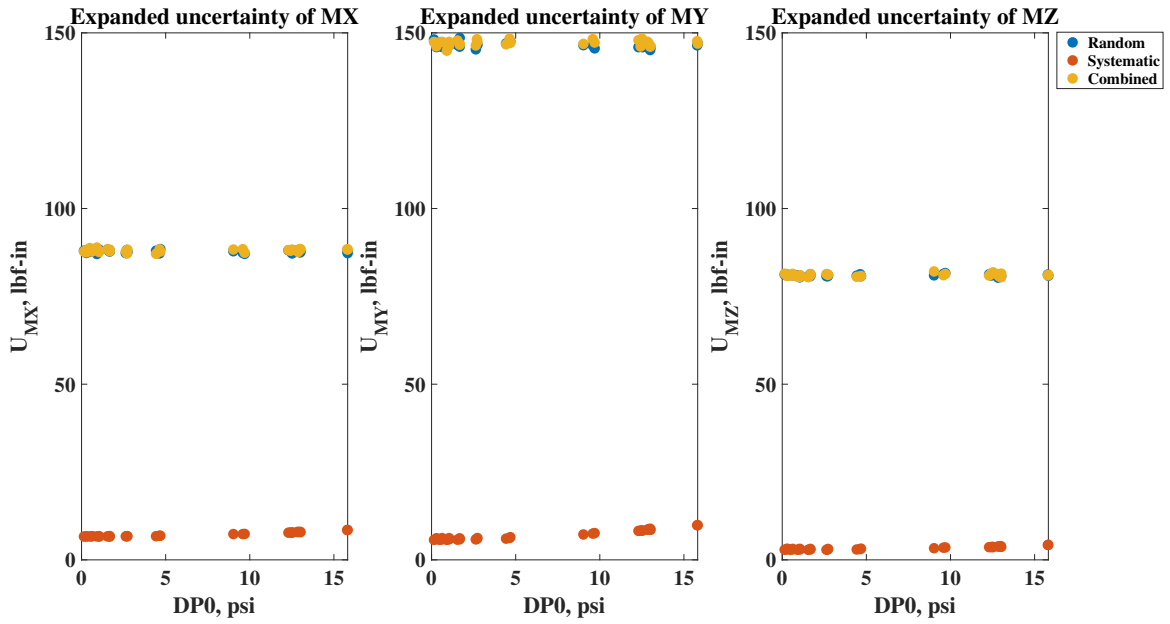


Figure 41: Expanded combined uncertainty in calculated moments

<i>DPO</i> [psi]	<i>FGY</i>			<i>FGZ</i>		
	<i>S_{FGY}</i> [lbf]	<i>B_{FGY}</i> [lbf]	<i>U_{FGY}</i> [lbf]	<i>S_{FGZ}</i> [lbf]	<i>B_{FGZ}</i> [lbf]	<i>U_{FGZ}</i> [lbf]
1.0	4.7	1.6	5.0	7.8	4.5	9.0
4.4	4.7	1.6	5.0	7.8	4.7	9.2
9.0	4.7	1.7	5.0	7.8	5.0	9.3
12.3	4.7	1.8	5.0	7.8	5.3	9.5
13.0	4.7	1.9	5.1	7.8	5.4	9.6
15.8	4.7	2.0	5.1	7.8	5.8	9.7

<i>DPO</i> [psi]	<i>MX</i>			<i>MY</i>			<i>MZ</i>		
	<i>S_{MX}</i> [lbf-in]	<i>B_{MX}</i> [lbf-in]	<i>U_{MX}</i> [lbf-in]	<i>S_{MY}</i> [lbf-in]	<i>B_{MY}</i> [lbf-in]	<i>U_{MY}</i> [lbf-in]	<i>S_{MZ}</i> [lbf-in]	<i>B_{MZ}</i> [lbf-in]	<i>U_{MZ}</i> [lbf-in]
1.0	88.1	6.7	88.4	146.5	6.0	146.6	80.9	3.1	81.0
4.4	88.1	6.7	88.4	146.5	6.2	146.6	80.9	3.0	81.0
9.0	88.1	7.3	88.4	146.5	7.2	146.7	80.9	3.3	81.0
12.3	88.1	7.7	88.4	146.5	8.3	146.7	80.9	3.6	81.0
13.0	88.1	7.9	88.5	146.5	8.5	146.7	80.9	3.7	81.0
15.8	88.1	8.5	88.5	146.5	9.9	146.8	80.9	4.3	81.0

Figure 42: Tabulated results for expanded random, systematic and combined uncertainty in *FGY*, *FGZ*, *MX*, *MY* and *MZ*

7.4 Uncertainty Sources

While Pareto charts and uncertainty percent contribution charts cannot be compiled for variables of interest in this analysis due to some non-Gaussian distributions when individual uncertainty sources are simulated, charts are included in this section showing high, moderate and low uncertainty contributors to combined uncertainties. These charts may be useful in determining which uncertainty sources are critical to parameters of interest, so efforts might be meaningfully focused on making consequential changes. These charts were compiled by plotting histograms of the combined uncertainty of each variable of interest (all sources propagated) and comparing to histograms of each uncertainty source individually propagated through the Monte Carlo code. Only uncertainty sources that contributed over 10% of the combined uncertainty are charted.

Figure 43 shows significant uncertainty sources contributing to combined uncertainty in P_0 , PT , DP_{25} , MX , MY , MZ and $M5ID$. Uncertainty sources contributed the same levels across all operating conditions simulated. Figures 44 and 45 show significant uncertainty sources contributing to combined uncertainty in NPR , FGY , and FGZ . Significant operating conditions that effect uncertainty sensitivity are charted for these variables of interest.

Uncertainty source	Variable of interest						
	u_{P_0}	u_{PT}	$u_{DP_{25}}$	u_{MX}	u_{MY}	u_{MZ}	u_{M5ID}
s_F				H	H	H	
$b_{P,ESP15}$	H						
$s_{P,ESP15}$	L						
$b_{P,ESP45}$		H					L
$s_{P,ESP45}$		L					L
$s_{DP_{25}}$			L				
s_{TT}							
$b_{P,ESP500}$							
$s_{P,ESP500}$							
b_{ASNOZZ}							
b_{PPSYX}							
s_{POSYX}				M			L
s_{SECSYX}				L	L	L	
$s_{ALS3SYX}$							
$b_{ASMESYX}$							
b_{Pbot}	M	L					
b_{ALS1}							
b_{AS}							
$b_{DP_{25}}$			H				H
b_{TT}							
b_{PPCAL}							
b_{POCAL}							
b_{SECCAL}							
$b_{ALS3CAL}$							
$b_{ASMECAL}$							

H	Source is a <i>high</i> contributor to uncertainty in VOI (changes to this source would definitely have an impact on uncertainty of interest, particularly if it is the sole "high" contributor)
M	Source is a <i>moderate</i> contributor to uncertainty in VOI (changes to this source may have a minor impact on uncertainty of interest)
L	Source is a <i>low</i> contributor to uncertainty in VOI (changes to this source would have a very small or negligible impact on uncertainty of interest)

Figure 43: Uncertainty sources and their levels of contribution to u_{P_0} , u_{PT} , $u_{DP_{25}}$, u_{MX} , u_{MY} , u_{MZ} , and u_{M5ID}

Uncertainty source	NPR	22.0	19.0	16.1	13.1	10.0	7.0	3.9	3.0	2.6	1.4	1.1
<i>S_F</i>												
<i>b_{P,ESP15}</i>		H	H	H	H	H	H	H	M	M	M	M
<i>S_{P,ESP15}</i>												
<i>b_{P,ESP45}</i>		L	L	L	L	L	M	H	H	H	H	H
<i>S_{P,ESP45}</i>								L	L	L	L	M
<i>S_{DP25}</i>												
<i>S_{TT}</i>												
<i>b_{P,ESP500}</i>												
<i>S_{P,ESP500}</i>												
<i>b_{ABNOZZ}</i>												
<i>b_{PPSYX}</i>												
<i>S_{P05YX}</i>												
<i>S_{SECSYX}</i>												
<i>S_{ALS3YX}</i>												
<i>b_{ASMESYX}</i>												
<i>b_{P04T}</i>		L	L	L	L	L	L	L	L	L	L	L
<i>b_{ALS1}</i>												
<i>b_{AS}</i>												
<i>b_{DP25}</i>												
<i>b_{TT}</i>												
<i>b_{PPCAL}</i>												
<i>b_{PCAL}</i>												
<i>b_{SECCAL}</i>												
<i>b_{ALS3CAL}</i>												
<i>b_{ASMICAL}</i>												

H
Source is a <i>high</i> contributor to uncertainty in VOI (changes to this source would definitely have an impact on uncertainty of interest, particularly if it is the sole "high" contributor)
M
Source is a <i>moderate</i> contributor to uncertainty in VOI (changes to this source may have a minor impact on uncertainty of interest)
L
Source is a <i>low</i> contributor to uncertainty in VOI (changes to this source would have a very small or negligible impact on uncertainty of interest)

Figure 44: Uncertainty sources and their levels of contribution to u_{NPR}

Uncertainty source	DP0 [psi]	FGY					FGZ				
		1.0	4.7	9.7	13.0	15.8	1.0	4.7	9.7	13.0	15.8
S_F		H	H	H	H	H	H	H	H	H	H
$b_{P,ESP15}$											
$S_{P,ESP15}$											
$b_{P,ESP45}$											
$S_{P,ESP45}$											
S_{DP25}											
S_{TT}											
$b_{P,ESP500}$											
$S_{P,ESP500}$											
b_{ASNOZZ}											
b_{PPSYX}		L	L	L	L	L	M	M	M	M	
S_{P05YX}		L	L	L	L	L	M	M	M	M	
S_{SECYX}		L	L	L	L	L	L	L	L	L	
$S_{ALS35YX}$											
$b_{ASMESYX}$											
b_{PBAR}											
b_{ALS1}											
b_{A5}											
b_{DP25}											
b_{TT}											
b_{PPCAL}											
b_{PPCAL}			L	L	L	L	L	L	M	M	
b_{SECCAL}											
$b_{ALS3CAL}$											
$b_{ASMECAL}$											

H
Source is a <i>high</i> contributor to uncertainty in VOI (changes to this source would definitely have an impact on uncertainty of interest, particularly if it is the sole "high" contributor)
M
Source is a <i>moderate</i> contributor to uncertainty in VOI (changes to this source may have a minor impact on uncertainty of interest)
L
Source is a <i>low</i> contributor to uncertainty in VOI (changes to this source would have a very small or negligible impact on uncertainty of interest)

Figure 45: Uncertainty sources and their levels of contribution to u_{FGY} and u_{FGZ}

7.5 Example results for WP, CDN, FG and CFG : Mass flow, discharge coefficient, gross thrust and thrust coefficient

An example of combined, systematic and random uncertainty results obtained for critical variables of interest FG, CFG, WP and CDN are presented in Figure 46.¹As has been extensively noted to this point, these results are only intended to provide an example of uncertainty outcomes based on a very specific ASME calibration. For this example, an ASME calibration using a nozzle size of 24in^2 was performed at various altitude conditions, then the system of Monte Carlo propagation codes were executed using a simulated customer test matrix similar to that of the calibration.

Since uncertainties in these variables have a high sensitivity to the ASME calibration, results should not be assumed to apply (even with matching configuration and set conditions), and should not be generalized or extrapolated. Uncertainty estimates for these critical variables can be made available to customers once an ASME calibration specifically catered to their test is performed. (Pre-test entry estimates can be provided upon request if sufficient data and information are available to support the request.)

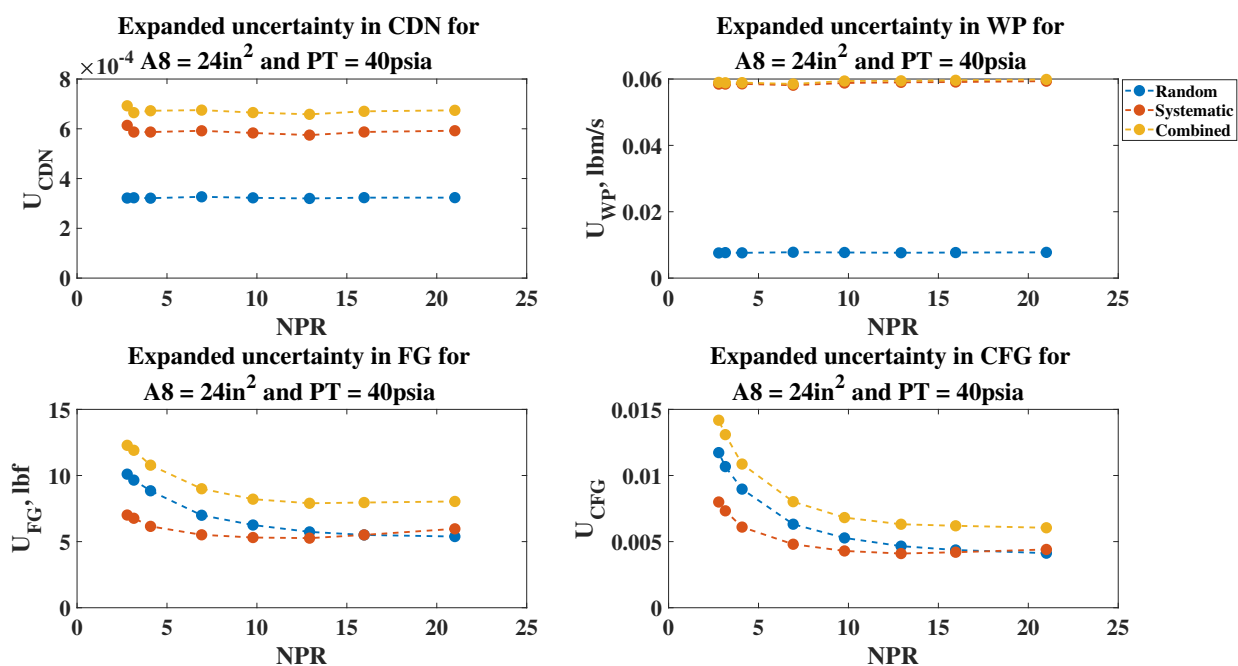


Figure 46: Example of expanded combined, random and systematic uncertainty in critical variables of interest^m

¹Estimates of $u_{CD5} = 1.3e - 4$ and $u_{CF5} = 5.0e - 4$ are used as prediction uncertainties from the ASME calibration, based on the specific calibration and data analysis used for this uncertainty propagation using methods presented in Section 6.2.5. Fossilized uncertainty from this specific ASME calibration also contributes to resulting uncertainties of interest as an artifact of other elemental uncertainties that were propagated through system of Monte Carlo codes. These estimates should also not be generalized.

^mUncertainty results for these variables are derived from a very specific ASME calibration simulation. They should not be extrapolated or generalized to apply to all facility conditions or nozzle sizes.

8 What-If Scenario

Once the uncertainty propagation codes are established, it is beneficial to use them as a tool to explore potential uncertainty improvement or cost-saving scenarios that do not compromise data quality. With minor adjustments to the existing simulation, information can be extracted regarding the degree of impact of such scenarios.

8.1 Push-Pull Calibration: Test Matrix Optimization

8.1.1 Scenario description

The current test matrix for the Push-Pull calibration involves sweeps of loads applied in nine different sets of combinations to obtain the thrust stand response characteristics. The main values of interest obtained are the slopes determined by performing a first-order fit of the response loads to the applied loads. Early on in this analysis, the facility researcher inquired about optimization of this test matrix. The question was, how many points are required during calibration to ensure quality results in the slopes but that might also provide a smaller test matrix which can be accomplished more quickly and cost effectively, without compromising uncertainty?

It is not at all uncommon for facilities to perform endpoint-only calibrations to identify sensitivity responses for thrust stands. In fact, the Propulsion Systems Laboratory (PSL) at NASA Glenn implements this approach for their Ormond thrust stand. In order to explore this scenario and quantify associated impact on uncertainty, three theoretical test matrices are proposed: a three-point calibration per load sequence (including full-load endpoints and a midpoint, for each of the nine load combinations: 27 total points), a six-point calibration (the three-point calibration, repeated twice: 54 total points), and the full calibration test matrix (which includes approximately 22-25 points per load combination: >200 total points).

These proposed test matrices were each run through the Monte Carlo simulation from beginning to end of the entire calibration sequence and test-time simulation to obtain comparative results. All systematic uncertainties were applied in these simulations, since the effect of the calibration is categorized as a fossilized systematic uncertainty, such that any errors present during the Push-Pull calibration have a trickle-down effect through all of the remaining calibrations and customer test. The results that follow, therefore, include the *total impact* of the size of the Push-Pull test matrix on customer test results.

8.1.2 Scenario results

The main variables of interest for this what-if scenario are the gross thrust, gross forces and moments, and the coefficient of thrust. Simulation results for calculated moments are shown for the three-point, six-point and full calibrations in Figures 47-49. Some non-negligible increases in systematic uncertainty in the calculated moments MY and MZ were noted with decrease in the size of the Push-Pull calibration test matrix. This may not be consequential, since the random uncertainty component of uncertainty in these variables of interest completely dwarf any systematic uncertainty contribution.

While this simulation did show a very slight increase of uncertainties in calculated forces using the proposed smaller test matrices, other contributors of systematic uncertainty have a much greater influence on the systematic uncertainty of these variables of interest. No appreciable differences in the uncertainty in gross thrust, the coefficient of thrust, nor in any of the gross directional forces were found with alteration of the Push-Pull calibration test matrix. We can conclude that for the purpose of thrust and force calculations, the smallest test matrix is completely adequate without compromising uncertainty in these parameters.

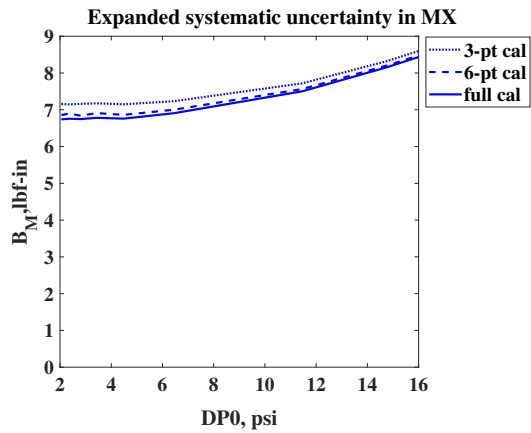


Figure 47: Expanded systematic uncertainty in *MX* for proposed Push-Pull calibration test matrices

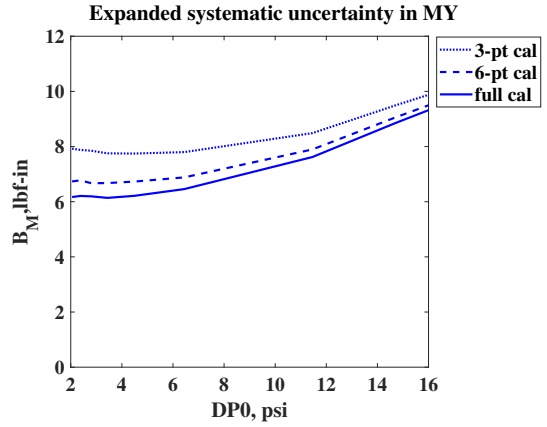


Figure 48: Expanded systematic uncertainty in *MY* for proposed Push-Pull calibration test matrices

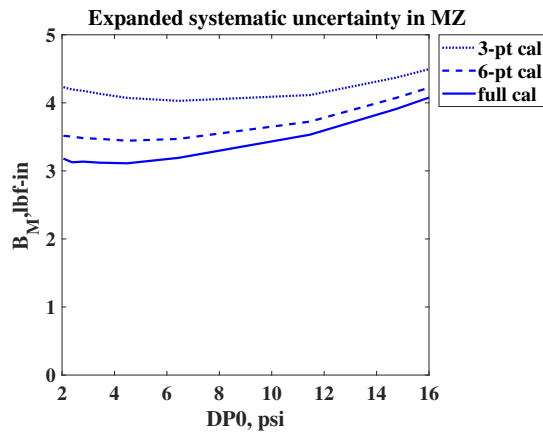


Figure 49: Expanded systematic uncertainty in *MZ* for proposed Push-Pull calibration test matrices

9 Conclusion

An uncertainty analysis was performed for the Advanced Nozzle Test Facility, CE-22, located at the NASA Glenn Research Center. All assumptions and elemental uncertainty estimates made for this analysis were detailed. The Monte Carlo method of propagating uncertainty was used to achieve uncertainty estimation of several facility calculated variables of interest.

Throughout this document, uncertainties were classified as random and systematic to aid facility personnel and researchers in determining which uncertainties are of interest for specific tests. Uncertainty sources were determined and elemental uncertainty estimates were made for all sources considered. Instrumentation uncertainties were estimated using MANTUS, a Microsoft Excel based tool tailored for modularized instrument systems to determine the combined uncertainty of an instrument measurement system. Random uncertainties were estimated using short-term observations collected by frequent facility users. Uncertainty of values predicted by regression fits were estimated using statistical analysis and were propagated whenever regressions were called on to predict values. All uncertainties considered in the analysis were propagated from the point of measurement through the instrumentation, data system, calibrations and final customer test data reduction sequence to obtain combined uncertainty results for several variables of interest. Random uncertainty results were analyzed and broken down so that a comprehensive understanding of driving random uncertainty sources could be determined.

Simulating the entire calibration sequence and customer test proved to be more difficult than anticipated. Due to the large number of measurements, uncertainty sources, calculations, uncertainty correlations within and between tests, and use of the Nelder-Mead minimizing function, the propagation code length was great and run-time was very high. To mitigate this, it was necessary to group some uncertainty sources and propagate multiple sources at once, limiting the discreteness in results that could be achieved. Also, some error distributions of calculated variables of interest had skewed or multimodal characteristics, making it impossible to create UPC charts. Driving factors to uncertainty were instead identified using visual inspection of histograms that were generated by propagating only individual or small groups of uncertainty sources at a time.

A scenario was developed and simulated to deduce its potential impact on uncertainty. These types of scenarios and exploration enable facility personnel to make educated improvements as they consider facility upgrades and plan future calibration and customer tests. One such scenario that was explored indicated there would be little to no impact on the uncertainty if endpoint-only loads were applied during the Push-Pull calibration test (instead of the current extensive test matrix), which would provide a time-saving technique without compromising uncertainty.

To continue refinement of uncertainty estimates in CE-22, it would be worthwhile to build some repeatability into ASME calibrations. Repeat data can be used to verify current random uncertainty results (or refine them as needed) by performing statistical analysis of directly calculated variables of interest such as *CDN* and *CFG*. Random uncertainty results deduced from uncertainty propagation can become inflated if there are unknown correlations that are not properly understood and accounted for. Additionally, due to the sensitivity of critical variables of interest to the ASME calibration and its specificity to each test program, facility personnel and the uncertainty team will continue to collaborate as ASME calibrations occur so that customers can be provided with accurate uncertainty estimates that directly pertain to their tests on an ongoing basis.

10 References

- [1] John D. Wolter. "Advanced Nozzle Test Facility Technical Guide". Technical guide, National Aeronautics and Space Administration, Document in progress.
- [2] Roger A. Werner and John D. Wolter. "Calibration for Thrust and Airflow Measurements in the CE-22 Advanced Nozzle Test Facility". Technical Memorandum NASA/TM-2010-216771, National Aeronautics and Space Administration, November 2010.
- [3] Kin C. Wong. "Derivation of the Data Reduction Equations for the Calibration of the Six-Component Thrust Stand in the CE-22 Advanced Nozzle Test Facility". Technical Memorandum NASA/TM-2003-212326, National Aeronautics and Space Administration, April 2003.
- [4] J. Stephens, E. Hubbard, J. Walter, and T. McElroy. "Uncertainty Analysis of the NASA Glenn 8x6 Supersonic Wind Tunnel". Contractor Report NASA/CR-2016-219411, National Aeronautics and Space Administration, 2016.
- [5] H. W. Coleman and W. G. Steele. *Experimentation, Validation and Uncertainty Analysis for Engineers*. John Wiley and Sons, Inc., Third edition, 2009.
- [6] Joint Committee for Guides in Metrology. "Evaluation of Measurement Data - Guide to the Expression of Uncertainty in Measurement". Guide JCGM 100:2008, International Organization for Standardization, 2008.
- [7] S. Castrup and H.T. Castrup. "Measurement Uncertainty Analysis Principles and Methods: NASA Measurement Quality Assurance Handbook - ANNEX 3". Handbook NASA HDBK 8739.19-3, National Aeronautics and Space Administration, 2010.

